Blocking Toxin Function and Modulating the Gut Microbiota: Caffeic Acid and its Derivatives as Potential Treatments for *Clostridioides difficile* Infection

Yan Guo[1#], Yong Zhang[2#], Guizhen Wang[3], Hongtao Liu[1], Jianfeng Wang[1], Xuming Deng[1], Liuqing He[4*], Jiazhang Qiu[1*]

[1] State Key Laboratory for Diagnosis and Treatment of Severe Zoonotic Infectious Diseases, Key Laboratory for Zoonosis Research of the Ministry of Education, College of Veterinary Medicine, Jilin University, Changchun, China.

[2] Center for Pathogen Biology and Infectious Diseases, State Key Laboratory for Zoonotic Diseases, The First Hospital of Jilin University, Changchun 130021, China.

[3] Measurement Biotechnique Research Center, College of Biological and Food Engineering, Jilin Engineering Normal University, Changchun 130052, China.

[4] Hunan Provincial Key Laboratory of Animal Intestinal Function and Regulation, Hunan International Joint Laboratory of Animal Intestinal Ecology and Health, Laboratory of Animal Nutrition and Human Health, College of Life Sciences, Hunan Normal University, Changsha, China.

#YG and YZ contributed equally to this work.

[*]Correspondence: Jiazhang Qiu (qiujz@jlu.edu.cn); Liuqin He (heliuqin@hunnu.edu.cn)

Abstract

Clostridioides difficile infection (CDI) is the leading cause of hospital-acquired diarrhea that seriously threatens public health. The disruption of normal gut microbiota by the use of broad-spectrum antimicrobial agents enables *C. difficile* to proliferate in the colon. The emergence and prevalence of hypervirulent *C. difficile* strains result in increased morbidity, mortality, and recurrence rates of CDI, thus creating a pressing need for novel therapeutics. The multi-domain toxins TcdA and TcdB are the primary determinants of CDI pathogenesis, rendering them ideal drug targets in the anti-virulence paradigm. In this study, we identified caffeic acid and its derivatives as active inhibitors of TcdB via a cell-based high-throughput phenotypic screening. Further mechanistic investigations revealed that caffeic acid phenethyl ester (CAPE) could directly bind to TcdB, thus suppressing InsP6-induced autoproteolysis and inhibiting glucosyltransferase activity. CAPE treatment remarkably reduces the pathology of CDI in a murine infection model in terms of alleviated diarrhea symptoms, decreased bacterial colonization, and relieved histopathological lesions. Moreover, CAPE treatment of C. difficile-challenged mice induces a remarkable increase in the diversity and composition of the gut microbiota (e.g., *Bacteroides*) and alterations of gut metabolites (e.g., adenosine, D-proline, and melatonin), which might partially contribute to the therapeutic outcomes of CAPE against CDI. Our results reveal the potential of CAPE as a therapeutic for the management of CDI, or CAPE might serve as a lead compound for the

45 development of antivirulence drugs targeting TcdB.

46

47 **Keywords:** *Clostridioides difficile*; toxin B; caffeic acid phenethyl ester; gut

48 microbiota; gut metabolites

49

Introduction

Clostridioides difficile (*C. difficile*) is an obligate anaerobic, spore-forming, gram-positive bacterial pathogen that is the most common cause of hospital-acquired and antibiotic-associated gastrointestinal diseases, including mild diarrhea and life-threatening pseudomembranous colitis [1, 2, 3]. In the United States, *C. difficile* is responsible for almost half a million infections and approximately 29,000 deaths per year, resulting in an estimated annual healthcare-associated cost of up to $4.8 billion [4, 5]. Importantly, the incidence, severity, mortality and healthcare costs of *C. difficile* infection (CDI) have dramatically increased in the 21st century, at least partially owing to the frequent use of antimicrobial agents and the emergence of hypervirulent strains (e.g., PCR ribotypes 027 and 078) [6, 7, 8]. Limited options are available for the treatment of CDI, while antibiotics including metronidazole, fidaxomicin and vancomycin, are the mainstays of clinical practice [9, 10]. However, antibiotic treatment is ineffective in more than 35% of CDI patients and can lead infection recurrence [11, 12]. Moreover, the rapid evolution of antibiotic resistance in *C. difficile* has further compromised the therapeutic efficacy of current treatment options [13]. Therefore, the high morbidity and mortality, high recurrence rates, and emergence of multiple antibiotic-resistant isolates have made this pathogen a major threat to public health; these factors highlight the urgent need for novel therapies.

C. difficile widely exists in the environment and in the intestinal tract of

72 humans and animals and is mainly transmitted via the fecal-oral route [14]. The
73 pathogenesis of CDI is correlated with the use of antibiotics, which impair the
74 structure and composition of the normal gut microbiota, thus allowing *C. difficile*
75 to proliferate in the colon [14]. Therefore, previous antibiotic therapy is the major
76 risk factor for the development of CDI. In the colon, the dormant spores of *C.*
77 *difficile* germinate into oxygen-sensitive vegetative cells that produce toxins and
78 cause symptoms of disease [15]. *C. difficile* secretes two large clostridial
79 exotoxins (TcdA and TcdB), which are directly responsible for the clinical
80 pathology of CDI [16, 17]. Epidemiological studies suggest that most disease-
81 causing *C. difficile* strains have genes that encode TcdB [18, 19]. TcdA and TcdB
82 have identical functional domains: a N-terminal glucosyltransferase catalytic
83 domain (GTD), a cysteine protease active domain (CPD), a transmembrane
84 domain (DRBD), and a C-terminal receptor binding domain (CROPs) [20]. When
85 secreted into the colon, both toxins are internalized by host cells through
86 receptor-mediated, clathrin-dependent endocytosis. Following a decrease in
87 endosomal pH, the toxins undergo conformational changes in the DRBD,
88 resulting in insertion of the toxin into the endosome membrane, pore formation,
89 and the release of the GTD and CPD domains into the cytosol. Then, CPD
90 binding with cytosolic inositol hexakisphosphate ($InsP_6$) activates its protease
91 activity, leading to the cleavage and release of the GTD. Eventually, the GTD
92 utilizes UDP-glucose to glucosylate Rho and/or Ras family GTPases, thus
93 disrupting GTPase signaling and resulting in deleterious effects, including

94 cytopathic “rounding”, dysregulation of the actin cytoskeleton, apoptosis, and
95 pyroptosis [1]. Although both toxins are cytotoxic to host cells, TcdB shows
96 greater toxicity than TcdA [21].

97 Disruption of the gut microbiota by antimicrobial agents results in high
98 recurrence rates, which limits the application of antimicrobial therapy for CDI [14].
99 Consequently, there is a critical need to develop nonantibiotic treatments for
100 CDI, either as standalone or augmented therapies. Importantly, strategies
101 targeting bacterial virulence factors, including toxins, are termed anti-virulence
102 strategies and have attracted interest in the 21st century [22]. Owing to its
103 essential role in *C. difficile* pathogenesis, TcdB has become an ideal target for
104 the development of anti-virulence drugs [23]. In this study, caffeic acid and a
105 series of its derivatives were found to inhibit TcdB-mediated cell rounding via
106 cell-based screening. Among these potential inhibitors, caffeic acid phenethyl
107 ester (CAPE) had the greatest inhibitory effect. Mechanistically, CAPE bound
108 to both full-length TcdB and the GTD fragment, leading to alterations in the
109 secondary structure. This interaction suppressed the $InsP_6$-mediated self-
110 cleavage of TcdB, as well as the enzymatic activity of GTD, thereby decreasing
111 the level of glucosylated Rac1 in TcdB-treated host cells and further inhibiting
112 the cytopathology and cytotoxicity of TcdB. Oral administration of CAPE
113 significantly protected against CDI in models of animal infection. In addition to
114 direct toxin inhibition, the therapeutic effect may also be attributed to CAPE-
115 induced alteration of the gut microbiota (e.g., *Bacteroides*) as well as gut

116 metabolites (e.g., adenosine, D-proline, and melatonin). Overall, our study
117 revealed that caffeic acid and its derivatives, particularly CAPE, may serve as
118 promising lead compounds for the development of anti-virulence drugs to treat
119 CDI.
120

121 **Results**

122 **CAPE inhibits cell rounding induced by TcdB**

123 TcdB can inactivate Rho GTPases via glucosylation, leading to the loss of
124 cytoskeletal structure and cell-rounding. Consequently, we utilized this
125 phenotype to identify potential TcdB inhibitors from 2076 chemicals, including
126 1515 FDA-approved drugs and 561 natural compounds. The minimal
127 concentration of recombinant His_6-TcdB (0.2 ng/mL) that induced 100% cell
128 rounding within 1 h was used for drug screening. This concentration of TcdB
129 was preincubated with 8 μg/mL of the individual compounds for 1 h before the
130 compounds were added to Vero cell cultures. At 1 h post-TcdB treatment, cell
131 morphology was visualized under a light microscope (**Figure 1A**). These
132 analyses allowed us to identify 22 candidate compounds with potent inhibitory
133 effects (**Figure 1B**). Interestingly, six out of the 22 compounds were caffeic acid
134 derivatives. Caffeic acid itself only slightly inhibited TcdB-induced cell rounding,
135 with a 50% inhibitory concentration (IC_{50}) of 527.5 μg/mL (**Table S1**). Notably,
136 except for rosmarinic acid, the IC_{50} values for the other screened caffeic acid
137 derivatives were less than 6 μg/mL, suggesting that these compounds potently

138 inhibited TcdB-mediated toxicity (**Table S1**). CAPE is the phenethyl alcohol
139 ester of caffeic acid and a main active component of propolis with broad
140 pharmacological properties, such as anticancer, anti-inflammatory, antiviral,
141 antibacterial, antifungal, antioxidant, and immunomodulatory activities [24]. As
142 CAPE has the lowest IC_{50} (3.0 μg/mL) among the active caffeic acid derivatives,
143 it was selected as the representative compound for subsequent investigations
144 (**Table S1**). After preincubation with increasing concentrations of CAPE, dose-
145 dependent inhibition of cell rounding was observed in both Vero and HeLa cells
146 (**Figure 1C**). In addition, we also determined whether inhibition of TcdB by
147 CAPE could lead to loss of toxin function *in vivo* using a murine systemic
148 intoxication model. A lethal dose of recombinant His_6-TcdB (30 ng) was
149 preincubated with either DMSO or CAPE (2 or 4 μg/mL) for 1 h at 37 °C,
150 followed by intraperitoneal injection into mice. Notably, all mice in the DMSO
151 group (n=10) died within 36 h after toxin injection. However, 100% of mice
152 pretreated with CAPE 4 (μg/mL) toxin survived at the monitoring endpoint (72
153 h) (n=10) (**Figure 1D**). Taken together, these data indicate that CAPE is a
154 potent toxin inhibitor of TcdB.

155 **CAPE decreases $InsP_6$-induced autoproteolysis of TcdB and inhibits the**
156 **enzymatic activity of GTD**

157 TcdB is a multi-domain containing toxin that induces toxicity in host cells
158 via an intricate and multistep mechanism. This mechanism involves (i) receptor-
159 mediated endocytosis, (ii) pore formation and subsequent membrane

160 translocation, (iii) autoproteolysis and release of GTD, and (iv) the glucosylation
161 of small GTPases (**Figure 2A**). To determine the mechanism by which CAPE
162 suppresses the cytotoxicity of TcdB, we first labeled full-length TcdB with Alexa
163 Fluor 488; then, the concentration of the endocytosed toxin was determined via
164 flow cytometry. Apparently, incubation of CAPE with TcdB did not significantly
165 affect its entry into host cells (**Figure 2B**). Next, we stained CAPE-treated cells
166 with LysoTracker, a fluorescent dye that accumulates in the acidic organelles of
167 live cells. In contrast to the vacuolar-type H+-ATPase (V-ATPase) inhibitor
168 bafilomycin A1 (Baf-A1), CAPE treatment did not alter the intensity of
169 LysoTracker fluorescence staining in either THP-1 or Caco-2 cells, suggesting
170 that inactivation of TcdB by CAPE is not due to changes in the pH of endosomal
171 compartments (**Figure 2C-D** and **Figure S1A-B**).

172 These observations indicate that CAPE might exert its effects after
173 membrane translocation. Indeed, preincubation of full-length TcdB with CAPE
174 blocked the $InsP_6$-induced autoproteolysis of TcdB, as revealed by the gradual
175 decrease in the production of released GTP, followed by the addition of
176 increasing amounts of CAPE *in vitro* (**Figure 2E-F**). Furthermore, we
177 determined the glucosyltransferase activity using recombinant GTD in the
178 absence or presence of different doses of CAPE. Strikingly, incubation with 2
179 μg/mL CAPE resulted in a significant reduction in GTD activity, whereas 32
180 μg/mL CAPE compromised 87.5% of the enzymatic activity (**Figure 2G**).
181 Importantly, in response to suppression of $InsP_6$-induced autoproteolysis and

182 GTD function, treatment of TcdB-challenged cells with CAPE markedly
183 decreased the level of glucosylated Rac1 in a dose-dependent manner (**Figure**
184 **2H-I**). Taken together, these results suggest that CAPE disrupts $InsP_6$-induced
185 autoproteolysis of TcdB and inhibits the enzymatic activity of GTD, thereby
186 decreasing the glucosylation of Rac1 and alleviating cell rounding.

187 **CAPE alters the secondary structure of full-length TcdB and GTD**

188 To further clarify the mechanisms used by CAPE to inactivate TcdB, we
189 determined the secondary structures of full-length TcdB and GTD in the
190 absence or presence of CAPE by circular dichroism spectroscopy. Apparently,
191 incubation of CAPE with full-length TcdB resulted in a significant increase in the
192 α-helix content (15.4% to 21.0%) and a concomitant decrease in the β-pleated
193 sheet content (34.5% to 20.9%) (**Figure 3A-B**). Similarly, the secondary
194 structure of GTD was markedly altered upon incubation with CAPE, with the
195 proportion of α-helices decreasing from 37.9% to 0.0% and the proportion of β-
196 pleated sheets decreasing from 37.2% to 10.9% (**Figure 3C-D**). Taken together,
197 these data suggest that CAPE may interact with full-length TcdB and GTD to
198 induce conformational changes, thus impairing their functions.

199 **CAPE directly interacts with full-length TcdB and GTD**

200 To investigate the potential interaction between CAPE and TcdB or GTD,
201 the binding constants were determined by surface plasmon resonance (SPR)
202 analysis. The results showed that CAPE has strong binding affinity with full-
203 length TcdB and GTD, and the KD values were 1.269×10^{-5} M and 1.007×10^{-3}

204 M, respectively (**Figure 4A-B**). These data demonstrate the direct interaction
205 between CAPE and full-length TcdB/GTD.

206 Next, we performed molecular docking and molecular simulation dynamics
207 analyses to investigate the interaction between CAPE and GTD (**Figure 5A**).
208 The results revealed that Leu265, Asp286, Thr465, Ile466, Leu519, and Trp520
209 in GTD were potential binding sites for CAPE (**Figure 5A**). The root mean
210 square deviation (RMSD) of the GTD/CAPE complex was stable over a 100 ns
211 period of simulation (**Figure 5B**). Further energy decomposition analysis
212 showed that the side chains of Leu265, Thr465, Leu519, and Trp520 of GTD
213 contributed to binding with CAPE via van der Waals interactions, among which
214 Trp520 had the highest binding energy (**Figure 5C**). Moreover, we mutated
215 each of the residues that were involved in binding and subsequently determined
216 their glucosyltransferase activities in the presence or absence of CAPE. The
217 enzymatic activities of these mutants were similar to that of wild-type GTD
218 (**Figure 5D**). Mutations in GTD_{L265A}, GTD_{T465A}, GTD_{I466A}, and GTD_{L519A} did not
219 affect the inhibitory effect of CAPE (**Figure 5E-I**). However, the inhibition of
220 GTD_{W520A} and GTD_{D286A} by CAPE was notably compromised (**Figure 5J-K**).

221 **CAPE treatment reduces the pathology of CDI in a murine model**

222 The abovementioned observation that CAPE suppresses the function of
223 TcdB prompted us to further evaluate the potential therapeutic effects of this
224 compound in CDI. To this end, we employed a well-established murine model
225 in which infected mice can develop symptoms resembling those observed in

human CDIs (25). First, cytotoxicity measurements revealed that the viability of both THP-1 and Vero cells was not affected by CAPE treatment (**Figure S2A-B**), thus indicating low toxicity. Mice were preconditioned with drinking water containing 0.5 g/L cefoperazone for 5 days, followed by normal drinking water for 2 days. After challenge with *C. difficile* BAA-1870 via gavage, mice were then treated daily with either vehicle or 30 mg/kg CAPE by gavage throughout the disease course (day 0 to day 5) (**Figure 6A**). Severe weight loss in *C. difficile*-infected mice was observed on days 2 and 3 post infection and was accompanied by diarrhea (**Figure 6B**). Notably, compared to the infection control group, CAPE treatment significantly increased the dry/wet weight ratio of the mouse feces, suggesting the alleviation of diarrhea symptoms (**Figure 6C**). Correspondingly, the weight loss of mice was relieved upon receiving CAPE (**Figure 6B**). Moreover, fecal pellets collected on day 3 were used to determine the bacterial burden. The results revealed that CAPE treatment significantly decreased the number of *C. difficile* CFUs (**Figure 6D**). On day 3 post-*C. difficile* infection, the colon was collected for histopathological analysis. Remarkably, *C. difficile*-infected mice exhibited conspicuous colon edema, epithelial cell injury and inflammatory factor infiltration (**Figure 6E**). In contrast, these histopathological lesions were significantly less common in mice administered CAPE (**Figure 6F**). Taken together, these data demonstrate the efficacy of CAPE in the treatment of CDI.

CAPE induces distinct microbiota changes in CAPE mice when compared

with model mice

Antibiotic-induced dysbiosis of the gut microbiota promotes the development of CDI [25]. Therefore, we next determined whether CAPE has any impact on gut microbial communities that may contribute to its therapeutic efficacy. To this end, on the 3rd day after *C. difficile* challenge, fecal samples from the model group and CAPE treatment group were collected and subjected to microbiota analysis via 16S rRNA gene sequencing. Remarkably, as reflected by the Venn diagram, CAPE treatment resulted in significant changes in the microbial composition compared to those in the model group, and only 16.42% of the operational taxonomic units (OTUs) were shared (**Figure 7A**). In addition, both the α- and β-diversity of the gut microbiota in CAPE-treated mice were significantly greater than those in model mice. Specifically, the increase in the Chao1 richness estimator of mice in the CAPE treatment group suggested a greater number of microbial species and increased evenness in the fecal samples (**Figure 7B-C**); the increase in the Shannon–Wiener diversity index and the Simpson diversity index reflected a significant increase in microbiota diversity (**Figure 7D-E**). Principal coordinate analysis (PCoA) revealed distinct confidence ellipses between the bacterial communities of the CAPE-treated group and the model group, thereby revealing substantial differences in their microbiota profiles (**Figure 7F**).

A comparative analysis was performed to examine changes at the phylum level following CAPE treatment. *Bacteroidota*, *Firmicutes,* and *Proteobacteria*

270 were the major constituents in both the CAPE treatment and model groups,
271 suggesting that the administration of CAPE did not significantly alter the mouse
272 microbiota at the phylum level (**Figure 7G**). Next, we compared the 10 most
273 abundant species at the genus level. Notably, CAPE treatment markedly
274 elevated the abundance of *Bacteroides* and decreased the abundance of
275 *Muribaculaceae* and *Parabacteroides* (**Figure 7H**). Leveraging linear
276 discriminant analysis of effect sizes (LEfSe), the microbiota was examined at
277 the genus level to identify bacteria exhibiting substantial differences in
278 abundance between the two cohorts (LDA score > 3.5). After CAPE treatment,
279 the relative abundance of *Bacteroides*, *Ruminococcus_gnavus_group*,
280 *Muribaculum* and *Faecalibaculum* OTUs notably increased, while that of
281 *Hungatella*, *Parasutterella* and *Muribaculaceae* OTUs significantly decreased
282 (**Figure 7I**). *Bacteroides*, *Muribaculum* and *Faecalibaculum* improve
283 colonization resistance to *C. difficile* [26, 27, 28]. Importantly, the abundance of
284 these bacterial species increased following CAPE treatment (**Figure 7J-L**). In
285 contrast, the abundance of *Parasutterella*, a bacterium that facilitates *C. difficile*
286 colonization [29], was reduced in mice receiving CAPE (**Figure 7M**). Taken
287 together, these findings suggest that CAPE treatment accelerates microbiota
288 recovery during CDI.

289 **CAPE alters the levels of gut metabolites in *C. difficile*-infected mice**

290 In addition to the crucial role of the gut microbiota in conferring colonization
291 resistance against *C. difficile*, gut microbiota-derived metabolites significantly

292 contribute to the disease process [30]. Metabolomic analysis was performed to
293 evaluate the effects of CAPE treatment on gut metabolites in mice. The PLS-
294 DA model exhibited significant separation of clusters between the model and
295 CAPE treatment groups (**Figure 8A**). Among the 1599 metabolites, 109
296 showed substantial differences in levels between the two groups. Specifically,
297 CAPE-treated mice exhibited 19 metabolites with upregulated expression and
298 50 metabolites with downregulated expression compared to those in the model
299 group (fold change > 1.5) (**Figure 8B**). Furthermore, KEGG enrichment
300 analysis revealed that the differentially abundant metabolites were significantly
301 enriched in the purine metabolism and bile secretion pathways (**Figure 8C**).
302 Adenosine is an endogenous purine nucleoside that binds to specific cell
303 surface receptors to exert anti-inflammatory effects at high concentrations [31].
304 Importantly, CAPE treatment of *C. difficile*-infected mice can increase the
305 adenosine concentration in the gut (**Figure 8D**), which might be attributed to its
306 inhibition of xanthine oxidase [32]. Similarly, the levels of uric acid, the final
307 product of purine metabolism, were markedly decreased in mice after receiving
308 CAPE (**Figure 8D**). An earlier study reported that increasing the gut adenosine
309 concentration with an adenosine deaminase inhibitor prevents *C. difficile* toxin
310 A-induced enteritis in mice [33]. Therefore, the increase in gut adenosine induced
311 by CAPE might play an important role in its therapeutic efficacy in CDI.

312 *C. difficile* predominantly utilizes sugars and amino acids for energy
313 production through various metabolic pathways, such as fermentation [34].

314 Notably, Stickland fermentation, a Clostridia-specific type of amino acid
315 fermentation, is associated with *C. difficile* pathogenesis [34]. D-proline is one of
316 the preferred nutrients used by *C. difficile* in the Stickland reaction and is critical
317 for its growth [35, 36]. Interestingly, treatment of *C. difficile*-infected mice with
318 CAPE significantly reduced gut D-proline levels (**Figure 8D**). In addition, the
319 metabolomics data also revealed a dramatic increase in the level of melatonin
320 (**Figure 8D**), which is a ubiquitous indolamine that was previously shown to
321 decrease the rate of recurrent CDI [37]. Consistently, quantification of the
322 melatonin content in mouse fecal supernatants using a melatonin detection kit
323 revealed elevated levels of melatonin in CAPE-treated mice (**Figure S3**).
324 Moreover, correlation analysis revealed a positive association between
325 *Faecalibaculum* abundance and melatonin levels (**Figure S4**). Taken together,
326 these results indicate that alterations in gut metabolites caused by CAPE
327 treatment might contribute to its therapeutic efficacy in CDI.

328 **Oral administration of melatonin alleviates the symptoms of CDI**

329 Next, we investigated whether any of the upregulated metabolites had a
330 direct influence on TcdB. To this end, we preincubated recombinant TcdB with
331 each of the selected metabolites prior to addition to the cell cultures.
332 Interestingly, treatment with TcdB and 100 μg/mL melatonin significantly
333 alleviated the cell death induced by this toxin (**Figure 9A**). This observation
334 prompted us to investigate the direct therapeutic potential of melatonin in CDI.
335 Therefore, *C. difficile*-infected mice were orally administered 200 mg/kg

336 melatonin at 24 h intervals. The weight changes and the dry/wet ratio of the
337 stool samples were monitored daily for three days. The results showed that
338 melatonin-treated mice displayed remarkable alleviation of diarrhea, as
339 manifested by notable improvements in weight recovery and a significant
340 increase in the dry/wet weight ratio on the 2nd and 3rd days after *C. difficile*
341 challenge (**Figure 9B-C**). Consistent with these observations, histopathological
342 assessment of colonic tissue sections also revealed attenuated colon damage
343 upon melatonin treatment (**Figure 9D-E**). Taken together, these data indicate
344 that a high dose of exogenous melatonin could protect mice from CDI and that
345 the CAPE-induced increase in endogenous melatonin might improve the
346 therapeutic outcome of patients with CAPE.
347

348 **Discussion**

349 *C. difficile* has become the prevalent agent of nosocomial diarrhea and
350 substantially threatens public health. In particular, the increase in morbidity and
351 mortality caused by the prevalence of hypervirulent and drug-resistant strains
352 has become a global concern [7]. In 2019, *C. difficile* was listed by the US Centers
353 for Disease Control and Prevention as an "urgent threat" that surpassed
354 methicillin-resistant *Staphylococcus aureus* (MRSA) and ESBL-producing
355 *Enterobacterales* [38]. *C. difficile* is a commensal bacterium that colonizes the
356 lower gastrointestinal tract [39]. CDI typically occurs in susceptible individuals
357 whose normal gut microbiota is disrupted by the administration of broad-

358 spectrum antibiotics [39]. Although CDI is considered an antibiotic-associated
359 disease, the current treatment for CDI still relies on antimicrobial drugs,
360 including metronidazole, fidaxomicin and vancomycin [9, 10]. Despite antibiotic
361 therapy, more than 35% of CDI patients are susceptible to recurrent infection,
362 which is primarily attributable to the intrinsic effects of antimicrobial agents,
363 which disrupt the microbiota [12]. In addition, long-term administration of
364 antibiotics promotes the selection of antibiotic-resistant subpopulations in the
365 gut, thus increasing the risk of infections caused by antibiotic-resistant and
366 opportunistic bacteria [40]. As a result, the development of nonantibiotic
367 therapeutics is needed for the treatment of CDI.

368 Indeed, numerous novel treatments for CDI are being investigated, among
369 which the anti-virulence strategy represents one of the most promising and
370 successful therapeutic approaches [22, 41]. Unlike antibiotics, which target
371 bacterial components that are critical for bacterial growth, anti-virulence drugs
372 aim to disarm pathogenic bacteria by neutralizing their virulence factors [42, 43].
373 Therefore, this strategy imposes less selective pressure that directs bacterial
374 evolution of antimicrobial resistance [43]. The disease progression of CDI is
375 strictly dependent on large clostridial toxins (TcdA and TcdB), as strains lacking
376 both toxins (i.e., A^-B^-) were completely avirulent and failed to induce any
377 discernable disease symptoms in a hamster model of infection [44]. Importantly,
378 epidemic *C. difficile* strains with increased morbidity and mortality rates produce
379 greater amounts of toxins [45]. Based on these premises, TcdA and TcdB are

380 considered ideal drug targets for CDI in the anti-virulence paradigm [46]. Indeed,
381 bezlotoxumab, a fully humanized monoclonal antibody that neutralizes TcdB,
382 was recently approved by the FDA and used in CDI patients to reduce the rate
383 of recurrence [47]. This achievement has encouraged researchers to develop
384 next-generation anti-virulence treatments. In particular, small molecule
385 inhibitors of toxin production and/or activity have attracted increasing interest
386 owing to their advantages in cost and the convenience of oral administration [41].
387 The multidomain architecture and mechanisms of action of clostridial toxins
388 have provided distinct options for blocking their toxicity. Indeed, previous efforts
389 have identified diverse inhibitors that act on distinct steps of intoxication, such
390 as the inhibition of toxin binding to cell receptors, the suppression of endosomal
391 maturation, and the inactivation of GTD or CPD activities [23, 48, 49, 50, 51]. Although
392 which approach is the best remains unknown, we believe that an inhibitor that
393 targets multiple steps of intoxication would be superior to those that act on a
394 single step. In this study, we identified a series of caffeic acid derivatives that
395 were potent inhibitors of TcdB via a phenotypic screen. Further mechanistic
396 study revealed that CAPE, the phenethyl alcohol ester of caffeic acid, could
397 block $InsP_6$-induced autoproteolysis of TcdB and inactivate its GTD function
398 (**Figure 10**). Moreover, CAPE treatment significantly protected against CDI in a
399 mouse model of infection. Our results suggested that caffeic acid derivatives,
400 particularly CAPE, are promising lead compounds for the development of anti-
401 virulence drugs that target TcdB. CAPE is a major component of propolis, a

402 natural bee-produced substance that has been used as a remedy for thousands
403 of years in Europe and Asia [52]. As a result, further investigations on the
404 therapeutic potential of propolis against CDI, either in combination with
405 standard therapy or as a single therapy, would be of great interest.

406 Antibiotic-induced gut microbiota dysbiosis is a major risk factor for CDI [53].
407 Thus, reconstituting the gut microbiota is a promising strategy for CDI therapy.
408 Fecal microbiota transplantation (FMT) is considered an effective CDI
409 therapeutic strategy and is widely used in clinical practice [54]. Despite the high
410 cure rate and increasing popularity of FMT, its safety remains controversial.
411 Another prominent advantage of anti-virulence drugs is that they allow
412 maintenance of the normal microbiota, which is of critical importance for the
413 treatment of CDI. Importantly, CAPE treatment of *C. difficile*-infected mice
414 restored the structure and composition of the microbiota (**Figure 10**). In
415 particular, the abundance of *Bacteroides*, a critical gut microbiota component
416 that is required for *C. difficile* resistance [26], was significantly elevated upon
417 CAPE treatment. Interestingly, *Bacteroides* were also predominant in CDI
418 patients administered RBX2660 (Rebyota), an FDA-approved fecal microbiota
419 product [55, 56]. The increased diversity of the gut microbiota might contribute to
420 the therapeutic effects of CAPE in CDI.

421 In addition to the microbiota, gut metabolites also play crucial roles in the
422 pathogenesis of CDI, either by promoting or suppressing disease progression
423 [30]. For example, bile acids and amino acids promote spore germination and

424 pathogenesis, while secondary bile acid and short-chain fatty acids aid in
425 colonization resistance and suppress spore germination [30]. In addition to
426 restoration of the gut microbiota, metabolomics analysis of mouse fecal
427 samples revealed dramatic alterations in gut metabolites upon CAPE treatment
428 (**Figure 10**). The differentially abundant metabolites were significantly enriched
429 in the purine metabolism and bile metabolism pathways. Remarkably, the level
430 of adenosine, an endogenous purine nucleoside that is released from cells
431 upon injury or inflammation, was dramatically increased in CAPE-treated mice.
432 In contrast, the amount of uric acid, the final product of purine metabolism, was
433 reduced. Previous studies showed that the increase in adenosine
434 concentrations caused by the inhibition of adenosine deaminase via EHNA
435 prevents *C. difficile* TcdA-mediated damage and inflammation [33]. This
436 protection might be a result of the anti-inflammatory effects of adenosine, which
437 rely on the activation of its receptors [57]. In addition, we observed a reduction in
438 the amount of D-proline, which is one of the preferred amino acids utilized by
439 *C. difficile* to generate energy through Stickland reactions [35]. Melatonin is a
440 ubiquitous indolamine that has broad biological activities [58]. Notably, we
441 detected a significantly increase in the amount of melatonin in the feces of mice
442 that were administered CAPE. Importantly, an earlier study demonstrated a
443 decreased risk of recurrent CDI in patients exposed to melatonin, possibly
444 owing to its antibacterial and anti-inflammatory activities [37]. In this study, we
445 found that oral administration of exogenous melatonin alleviated the symptoms

446 of CDI in a mouse model of infection. Although determining the exact
447 mechanism will require further investigation, we propose that the melatonin-
448 mediated inhibition of TcdB intoxication observed in this study might contribute
449 to its therapeutic effect. Taken together, these results indicate that the
450 alterations in gut metabolites caused by CAPE might also contribute to
451 treatment outcomes for CDI patients.
452

453 **Methods**

454 **Cell lines**

455 All cell lines (HeLa, Caco-2, Vero, HEK293T and THP-1) were obtained
456 from ATCC (Manassas, VA). HeLa, Caco-2, Vero and HEK293T cells were
457 cultured in Dulbecco's modified Eagle's medium (DMEM) (Invitrogen, Carlsbad,
458 CA) supplemented with 10% fetal bovine serum (FBS) (Invitrogen) and 1% (w/v)
459 penicillin–streptomycin. THP-1 cells were cultured in Roswell Park Memorial
460 Institute (RPMI) 1640 medium (Invitrogen) supplemented with 10% FBS and 1%
461 (w/v) penicillin–streptomycin. All cell lines were cultured at 37 °C in a 5% CO_2
462 atmosphere.

463 **Bacterial strains and reagents**

464 *C. difficile* BAA-1870 (kindly provided by Aiwu Wu, Guangzhou Medical
465 University) was cultured in brain-heart infusion broth (BHI). The compounds
466 were identified from two main sources: FDA-approved drugs obtained from
467 ApexBio Technology (Houston, TX, USA) and small molecule natural

468 compounds obtained from Chengdu Ruifensi Biotechnology Co., Ltd. (Chengdu,
469 China). LysoTracker Red DND-99, kanamycin, and cefoperazone sodium were
470 purchased from Dalian Meilun Biotechnology Co., Ltd. (Dalian, China).

471 **Mice**

472 Male C57BL/6 mice aged 6-8 weeks were purchased from Liaoning
473 Changsheng Biotechnology Co., Ltd., and housed in a specific pathogen-free
474 (SPF) facility. The mice lived in a controlled environment with a temperature of
475 23±2 °C and a humidity of 55±10 °C. Prior to infection, the mice were
476 acclimated to the environment for a minimum of one week. All mouse
477 experiments were approved by the Jilin University Institutional Animal Care
478 Committee, Jilin University and strictly conducted according to the guidelines
479 of this committee (SY202309036).

480 **Protein expression and purification**

481 The expression and purification of full-length TcdB were conducted
482 following the method described by *Yang* et al. [59]. In brief, *Bacillus megaterium*
483 harboring pHis1522-TcdB was inoculated into LB media supplemented with a
484 final concentration of 10 μg/mL tetracycline. Once the $OD600_{nm}$ reached
485 approximately 0.3, xylose (0.5% w/v) was added to induce protein expression
486 at 37 °C for 16 h. Then, 100 mL of the bacterial cells was harvested by
487 centrifugation, resuspended in 5 mL of lysis buffer containing 20 mM imidazole,
488 300 mM NaCl, 20 mM NaH_2PO_4, 500 μM EDTA, and protease inhibitor cocktail
489 (adjusted to pH 8.0), and subjected to sonication. The cell lysate was then

490 centrifuged at 13,400 × g for 20 min to remove cell debris. The TcdB protein
491 was purified using nickel column affinity chromatography. The purity of the
492 protein was confirmed by SDS–PAGE, and the protein was subsequently
493 dialyzed against buffer containing 10% glycerol, 20 mM Tris (pH 7.5), and 150
494 mM NaCl. After the protein concentration was determined, the purified TcdB
495 protein was aliquoted and stored at -80 °C for further use.

496 For the purification of GTD, amplified DNA products were inserted into
497 pET28a (Novagen), and the *Escherichia coli* (*E. coli*) strain BL21 (DE3) was
498 used for the expression and purification of GTD. Transformed *E. coli* pET28a-
499 GTD was cultured in Luria–Bertani (LB) medium supplemented with 10 μg/mL
500 kanamycin. Once the OD600 reached 0.6, the expression of proteins was
501 induced with 0.2 mM isopropyl-β-d-thiogalactoside (IPTG) overnight at 18 °C.
502 The bacterial cells were then harvested by centrifugation and subjected to
503 sonication. The cell lysate was then centrifuged at 13,400 × g for 20 min to
504 remove cell debris. GTD protein was purified using nickel affinity
505 chromatography and dialyzed in buffer containing 10% glycerol, 20 mM Tris (pH
506 7.5), and 150 mM NaCl. The GTD mutants were introduced into pET28a-GTD
507 using the Quick Change Site-Directed Mutagenesis Kit (Stratagene, San Diego,
508 CA, USA) with the primers listed in **Table S2.** The subsequent purification was
509 performed using the same procedure as described for wild-type GTD.

510 **Cell rounding assay**

511 Vero or HeLa cells were seeded in 96-well sterile plates using serum-free

512 DMEM overnight, and the compounds were preincubated with TcdB for 1 h.
513 After incubation, the TcdB-compound complex was added to cells for 1 h at
514 37 °C. The cell morphology was visualized under a light microscope.

515 **LysoTracker assay**

516 The pH of endosomes was determined by LysoTracker Red DND-99.
517 Caco-2 or THP-1 cells in complete DMEM were seeded in 96-well sterile plates
518 overnight. The media was changed to serum-free DMEM for 1 h, and CAPE
519 was preincubated with TcdB for 1 h, followed by addition to the cells and
520 incubation for 2 h. Baf-A1 served as a control. After incubation, LysoTracker
521 and Hoechst dyes were added and the cells were incubated for 1 h. Excess dye
522 was removed by changing the media, and alterations in lysosomal red intensity
523 were documented using a fluorescence microscope.

524 ***In vitro* TcdB autoprocessing assay**

525 The self-cleavage ability of TcdB primarily depends on its cysteine protease
526 activity. CAPE (1-16 μg/mL) was preincubated with TcdB for 1 h, followed by
527 the addition of $InsP_6$ and incubation at 37 °C for 6 h. Subsequently, loading
528 buffer was added for SDS–PAGE analysis, and the results were visualized
529 using Coomassie Brilliant Blue staining.

530 **Rac1 glucosylation assay**

531 HEK293T cells were seeded into a 6-well plate. The next day, TcdB and
532 different concentrations of CAPE (4-32 μg/mL) were added to cells. After 2 h,
533 the cells were harvested, lysed using lysis buffer, and subjected to

534 centrifugation at 13,400 × g for 10 min to collect the supernatant. The collected
535 supernatant was then mixed with loading buffer and subjected to SDS–PAGE
536 followed by western blot analysis. The glycosylation level of Rac1 was
537 evaluated by determining the levels of non-glycosylated Rac1 (BD Biosciences,
538 Mississauga, ON) and total Rac1 (Abcam).

539 **UDP-Glo^{TM} UDP-glucose hydrolase assay**

540 GTD activity was assessed according to the manufacturer's instructions. A
541 total volume of 16 μL, consisting of 100 nM GTD, various concentrations of
542 CAPE and glucosylation buffer, was prepared. Four microliters of UDP-glucose
543 at a final concentration of 25 μM was added to the mixture, which was then
544 allowed to react at room temperature for 15 min. To stop the reaction, 10 μL of
545 the reaction mixture was removed and placed in a white polystyrene 96-well
546 plate containing 10 μL of UDP detection reagent. The reaction took place at
547 room temperature for 1 h. The luminescence value was measured at a 750 ms
548 integral, and the GTD activity was determined based on these measurements.

549 **Circular dichroism (CD) spectroscopy**

550 CD spectra of TcdB, TcdB-CAPE, GTD, and GTD-CAPE were obtained
551 using a CD spectrophotometer (MOS-500; Bio-Logic, France). TcdB or GTD at
552 a concentration of 0.2 mg/mL was incubated with 32 μg/mL CAPE. Changes in
553 the secondary structure of TcdB or GTD were assessed at room temperature
554 using a quartz cuvette with an optical path length of 1 mm. The scan wavelength
555 range was set from 190 to 250 nm with a resolution of 0.2 nm and a bandwidth

556 of 1 nm. The secondary structures of TcdB, TcdB-CAPE, GTD, and GTD-CAPE
557 were analyzed using the BeStSel web server.

558 **Molecular docking**

559 CAPE was obtained as a ligand from PubChem, and its topology was
560 generated using AmeberTools. The crystal structure of GTD was retrieved from
561 the Protein Data Bank (PDB) and processed using AutoDockTools. Docking
562 calculations were performed using AutodockVina, and molecular dynamics
563 simulations were carried out using Gromacs 2020.6. The RMSD of the receptor
564 and ligand was monitored to assess conformational changes during the binding
565 process. The interaction energy was analyzed using the Poisson-Boltzmann
566 surface area (MM-PBSA) method, which is a molecular mechanics approach.

567 **Flow cytometry**

568 Flow cytometry was used to quantify the cellular uptake of TcdB via
569 endocytosis. To facilitate detection, full-length TcdB was labeled with Alexa
570 Fluor®488 NHS Ester (Yeasen Biotechnology Co., Ltd., Shanghai, China). Prior
571 to cell treatment, Alexa Fluor 488-TcdB was preincubated with CAPE at a
572 concentration of 32 μg/mL for 30 min. The treated solution was then added to
573 Caco-2 cells and incubated for 1 h at 37 °C. Following three washes with
574 phosphate-buffered saline (PBS), the Caco-2 cells were collected, and the
575 fluorescence signal was measured using flow cytometry.

576 **Cytotoxicity assay**

577 Vero or THP-1 cells were plated into 96-well plates. The next day, different

578 concentrations of CAPE were prepared by diluting them in DMEM and adding
579 them to the cells. After incubation at 37 °C for 3 h, the viability of cells was
580 assessed using a Cell Counting Kit-8 (CCK-8) (Beyotime Biotechnology Co.,
581 Shanghai, China) according to the manufacturer's instructions.

582 **Biacore analysis**

583 The affinity analysis of TcdB or GTD with CAPE was conducted using a
584 Biacore T100 device (Biacore Inc., Uppsala, Sweden) according to the
585 manufacturer's protocol. A CM5 chip (General Electric Company, GE) was
586 utilized to immobilize the TcdB or GTD proteins. Various concentrations of
587 CAPE were injected, and all steps were performed in running buffer consisting
588 of 5% DMSO in PBS-P20 (GE). Evaluation version 3.1 software provided by
589 Biacore and the 1:1 Langmuir combined model were employed for data analysis.

590 **Mouse infection model**

591 For the acute toxicity model, after pretreatment of TcdB with CAPE (2 or 4
592 μg/mL) for 1 h, the mice were intraperitoneally injected with a complex of TcdB-
593 solvent or TcdB-CAPE (30 ng of TcdB per mouse). The survival of mice was
594 observed for 72 h.

595 For the CDI model, mice were given cefoperazone (0.5 g/L) in their drinking
596 water for 5 days (from day -7 to day -2), followed by switching to sterilized water
597 for 2 days. On day 0, the mice were challenged with 1×10^8 colony-forming
598 units (CFUs) of *C. difficile* BAA-1870 (Ribotype 027) by oral gavage. For the
599 CAPE or melatonin treatment group, mice were treated with CAPE (30 mg/kg

600 by oral gavage) or melatonin (200 mg/kg by oral gavage) every day after *C.*
601 *difficile* challenge. The weight loss and fecal state of the mice were monitored
602 daily. Fecal samples were collected on days 0-3 to evaluate the stool water
603 content as a marker of diarrhea. Additionally, fecal samples on day 3 were
604 collected to assess *C. difficile* colonization. Colonic tissues were collected on
605 day 3 post infection, stained with hematoxylin and eosin (H&E) and scored as
606 previously described [60].

607 Fecal samples were collected on day 3 post infection, frozen in liquid
608 nitrogen and transferred to the laboratory with dry ice for 16S rRNA sequencing
609 and untargeted metabolomics analysis (Novogene Bioinformatics Technology
610 Co., Ltd., Tianjin, China). The melatonin level in mouse stool supernatant was
611 determined using the Mouse MT (Melatonin) ELISA Kit (Sangon Biotechnology
612 Co., Ltd., Shanghai, China).

613 **Statistical analysis**

614 Western blot densitometry and LysoTracker fluorescence intensity were
615 measured using ImageJ software (NIH, Bethesda, MD, USA). Statistical
616 analysis was performed using GraphPad Prism 9.0 (GraphPad Software, USA).
617 Unpaired two-tailed Student's t tests were used for comparing two groups, and
618 one-way analysis of variance (ANOVA) was used for analyzing data from more
619 than three groups. The statistical significance was determined using the log-
620 rank (Mantel–Cox) test (survival rates) and Mann–Whitney U test (tissue
621 bacterial load) *in vivo*. All the data are expressed as the mean ± standard

622 deviation (SD). * indicates p <0.05 and ** indicates p <0.01.

623

624 **Acknowledgments**

625 The authors thank Professor Aiwu Wu (Guangzhou Medical University) for
626 the *C. difficile* BAA-1870 strain and Professor Hanping Feng (Tufts University)
627 for the pHis1522-TcdB plasmid. This work was supported by The National Key
628 Research & Development Program of China (2021YFD1801000), the Natural
629 Science Foundation of Jilin Province (20230101142JC and 20240101282JC),
630 and The Fundamental Research Funds for the Central Universities.

631

632 **Author contributions**

633 Y Guo., LQ He and JZ Qiu designed the study and wrote the manuscript.
634 Y Guo, Y Zhang, GZ Wang and HT Liu conducted experiments. JF Wang, XM
635 Deng, LQ He and JZ Qiu supervised the study and revised the manuscript. All
636 authors read and approved the final manuscript. JZ Qiu and LQ He are
637 responsible for the overall content as the guarantor.

638

639 **Disclosure statement**

640 No potential conflict of interest was reported by the author (s).

641

642 **Data availability**

643 All 16S rRNA gene sequencing data generated and analyzed during the

644 current study were deposited in the Sequence Read Archive (SRA) under the
645 BioProject accession number PRJNA1100298. Untargeted metabolomics data
646 are available via Metabolights with the identifier MTBLS9938.
647
648

References

1. Smits WK, Lyras D, Lacy DB, Wilcox MH, Kuijper EJ. Clostridium difficile infection. *Nat Rev Dis Primers* **2**, 16020 (2016).

2. Miller BA, Chen LF, Sexton DJ, Anderson DJ. Comparison of the burdens of hospital-onset, healthcare facility-associated Clostridium difficile Infection and of healthcare-associated infection due to methicillin-resistant Staphylococcus aureus in community hospitals. *Infect Control Hosp Epidemiol* **32**, 387-390 (2011).

3. Kelly CP, LaMont JT. Clostridium difficile--more difficult than ever. *N Engl J Med* **359**, 1932-1940 (2008).

4. Dubberke E. Clostridium difficile infection: the scope of the problem. *J Hosp Med* **7 Suppl 3**, S1-4 (2012).

5. Lessa FC*, et al.* Burden of Clostridium difficile infection in the United States. *N Engl J Med* **372**, 825-834 (2015).

6. Goorhuis A*, et al.* Emergence of Clostridium difficile infection due to a new hypervirulent strain, polymerase chain reaction ribotype 078. *Clin Infect Dis* **47**, 1162-1170 (2008).

7. He M*, et al.* Emergence and global spread of epidemic healthcare-associated Clostridium difficile. *Nat Genet* **45**, 109-113 (2013).

8. Clements AC, Magalhaes RJ, Tatem AJ, Paterson DL, Riley TV. Clostridium difficile PCR ribotype 027: assessing the risks of further worldwide spread. *Lancet Infect Dis* **10**, 395-404 (2010).

9. Cornely OA*, et al.* Fidaxomicin versus vancomycin for infection with Clostridium difficile in Europe, Canada, and the USA: a double-blind, non-inferiority, randomised controlled trial. *Lancet Infect Dis* **12**, 281-289 (2012).

10. Bingley PJ, Harding GM. Clostridium difficile colitis following treatment with metronidazole and vancomycin. *Postgrad Med J* **63**, 993-994 (1987).

11. Feuerstadt P, Theriault N, Tillotson G. The burden of CDI in the United States: a multifactorial challenge. *BMC Infect Dis* **23**, 132 (2023).

12. Hopkins RJ, Wilson RB. Treatment of recurrent Clostridium difficile colitis: a narrative review. *Gastroenterol Rep (Oxf)* **6**, 21-28 (2018).

13. Spigaglia P, Mastrantonio P, Barbanti F. Antibiotic Resistances of Clostridium difficile. *Adv Exp Med Biol* **1050**, 137-159 (2018).

14. Seekatz AM, Young VB. Clostridium difficile and the microbiota. *J Clin Invest* **124**, 4182-4189 (2014).

15. Paredes-Sabja D, Shen A, Sorg JA. Clostridium difficile spore biology: sporulation, germination, and spore structural proteins. *Trends Microbiol* **22**, 406-416 (2014).

16. Lyras D*, et al.* Toxin B is essential for virulence of Clostridium difficile. *Nature* **458**, 1176-1179 (2009).

17. Kuehne SA, Cartman ST, Heap JT, Kelly ML, Cockayne A, Minton NP. The role of toxin A and toxin B in Clostridium difficile infection. *Nature* **467**, 711-713 (2010).

18. Carter GP*, et al.* Defining the Roles of TcdA and TcdB in Localized Gastrointestinal Disease, Systemic Organ Damage, and the Host Response during Clostridium difficile Infections. *mBio* **6**, e00551 (2015).

19. Drudy D, Fanning S, Kyne L. Toxin A-negative, toxin B-positive Clostridium difficile. *Int J Infect Dis* **11**, 5-10 (2007).

20. Chen P*, et al.* Structure of the full-length Clostridium difficile toxin B. *Nat Struct Mol Biol* **26**, 712-719 (2019).

21. Orrell KE, Melnyk RA. Large Clostridial Toxins: Mechanisms and Roles in Disease. *Microbiol Mol Biol Rev* **85**, e0006421 (2021).

22. Rasko DA, Sperandio V. Anti-virulence strategies to combat bacteria-mediated disease. *Nat Rev Drug Discov* **9**, 117-128 (2010).

23. Tam J, Beilhartz GL, Auger A, Gupta P, Therien AG, Melnyk RA. Small molecule inhibitors of Clostridium difficile toxin B-induced cellular damage. *Chem Biol* **22**, 175-185 (2015).

24. Balaha M, De Filippis B, Cataldi A, di Giacomo V. CAPE and Neuroprotection: A Review. *Biomolecules* **11**, (2021).

25. Garland M*, et al.* The Clinical Drug Ebselen Attenuates Inflammation and Promotes Microbiome Recovery in Mice after Antibiotic Treatment for CDI. *Cell Rep Med* **1**, (2020).

26. Li X*, et al.* A strain of Bacteroides thetaiotaomicron attenuates colonization of Clostridioides difficile and affects intestinal microbiota and bile acids profile in a mouse model. *Biomed Pharmacother* **137**, 111290 (2021).

27. Kienesberger B*, et al.* (S)-Reutericyclin: Susceptibility Testing and In Vivo Effect on Murine Fecal Microbiome and Volatile Organic Compounds. *Int J Mol Sci* **22**, (2021).

28. Khanna S*, et al.* Gut microbiome predictors of treatment response and recurrence in primary Clostridium difficile infection. *Aliment Pharmacol Ther* **44**, 715-727 (2016).

29. Dong D*, et al.* Effects of intestinal colonization by Clostridium difficile and Staphylococcus aureus on microbiota diversity in healthy individuals in China. *BMC Infect Dis* **18**, 207 (2018).

30. Gurung B, Stricklin M, Wang S. Gut Microbiota-Gut Metabolites and Clostridioides difficile Infection: Approaching Sustainable Solutions for Therapy. *Metabolites* **14**, (2024).

31. Cronstein BN. Adenosine, an endogenous anti-inflammatory agent. *J Appl Physiol (1985)* **76**, 5-13 (1994).

32. Yong T*, et al.* Caffeic acid phenethyl ester alleviated hypouricemia in hyperuricemic mice through inhibiting XOD and up-regulating OAT3. *Phytomedicine* **103**, 154256 (2022).

33. de Araujo Junqueira AF*, et al.* Adenosine deaminase inhibition prevents Clostridium difficile toxin A-induced enteritis in mice. *Infect Immun* **79**, 653-662 (2011).

34. Neumann-Schaal M, Jahn D, Schmidt-Hohagen K. Metabolism the Difficile Way: The Key to the Success of the Pathogen Clostridioides difficile. *Front Microbiol* **10**, 219 (2019).

35. Bouillaut L, Self WT, Sonenshein AL. Proline-dependent regulation of Clostridium difficile Stickland metabolism. *J Bacteriol* **195**, 844-854 (2013).

36. Jackson S, Calos M, Myers A, Self WT. Analysis of proline reduction in the nosocomial pathogen Clostridium difficile. *J Bacteriol* **188**, 8487-8495 (2006).

37. Sutton SS, Magagnoli J, Cummings TH, Hardin JW. Melatonin as an Antimicrobial Adjuvant and Anti-Inflammatory for the Management of Recurrent Clostridioides difficile Infection. *Antibiotics (Basel)* **11**, (2022).

38. 2019 AR Threats Report. (2019). [Available from: https://www.cdc.gov/drugresistance/biggest-threats.html].

39. Abbas A, Zackular JP. Microbe-microbe interactions during Clostridioides difficile infection. *Curr Opin Microbiol* **53**, 19-25 (2020).

40. Raplee I*, et al.* Emergence of nosocomial associated opportunistic pathogens in the gut microbiome after antibiotic treatment. *Antimicrob Resist Infect Control* **10**, 36 (2021).

41. Beilhartz GL, Tam J, Melnyk RA. Small Molecules Take A Big Step Against Clostridium difficile. *Trends Microbiol* **23**, 746-748 (2015).

42. Ranftler C*, et al.* Binding and neutralization of C. difficile toxins A and B by purified clinoptilolite-tuff. *PLoS One* **16**, e0252211 (2021).

43. Zucca M, Scutera S, Savoia D. Novel avenues for Clostridium difficile infection drug discovery. *Expert Opin Drug Discov* **8**, 459-477 (2013).

44. Kuehne SA, Collery MM, Kelly ML, Cartman ST, Cockayne A, Minton NP. Importance of toxin A, toxin B, and CDT in virulence of an epidemic Clostridium difficile strain. *J Infect Dis* **209**, 83-86 (2014).

45. Warny M*, et al.* Toxin production by an emerging strain of Clostridium difficile associated with outbreaks of severe disease in North America and Europe. *Lancet* **366**, 1079-1084 (2005).

46. Stewart D, Anwar F, Vedantam G. Anti-virulence strategies for Clostridioides difficile infection: advances and roadblocks. *Gut Microbes* **12**, 1802865 (2020).

47. Deeks ED. Bezlotoxumab: A Review in Preventing Clostridium difficile Infection Recurrence. *Drugs* **77**, 1657-1663 (2017).

48. Bender KO*, et al.* A small-molecule antivirulence agent for treating Clostridium difficile infection. *Sci Transl Med* **7**, 306ra148 (2015).

49. Chan H*, et al.* Vitamin D(3) and carbamazepine protect against

824 Clostridioides difficile infection in mice by restoring macrophage
825 lysosome acidification. *Autophagy* **18**, 2050-2067 (2022).
826
827 50. Tam J*, et al.* Host-targeted niclosamide inhibits C. difficile virulence and
828 prevents disease in mice without disrupting the gut microbiota. *Nat*
829 *Commun* **9**, 5233 (2018).
830
831 51. Tam J*, et al.* Intestinal bile acids directly modulate the structure and
832 function of C. difficile TcdB toxin. *Proc Natl Acad Sci U S A* **117**, 6792-
833 6800 (2020).
834
835 52. Tek NA, Senture SA, Ersoy N. Is Propolis a Potential Anti-Obesogenic
836 Agent for Obesity? *Curr Nutr Rep*, (2024).
837
838 53. Schubert AM, Sinani H, Schloss PD. Antibiotic-Induced Alterations of the
839 Murine Gut Microbiota and Subsequent Effects on Colonization
840 Resistance against Clostridium difficile. *mBio* **6**, e00974 (2015).
841
842 54. van Nood E*, et al.* Duodenal infusion of donor feces for recurrent
843 Clostridium difficile. *N Engl J Med* **368**, 407-415 (2013).
844
845 55. Lee C*, et al.* Safety of fecal microbiota, live-jslm (REBYOTA()) in
846 individuals with recurrent Clostridioides difficile infection: data from five
847 prospective clinical trials. *Therap Adv Gastroenterol* **16**,
848 17562848231174277 (2023).
849
850 56. Gonzales-Luna AJ, Carlson TJ, Garey KW. Review Article: Safety of Live
851 Biotherapeutic Products Used for the Prevention of Clostridioides difficile
852 Infection Recurrence. *Clin Infect Dis* **77**, S487-S496 (2023).
853
854 57. Cavalcante IC*, et al.* Effect of novel A2A adenosine receptor agonist ATL
855 313 on Clostridium difficile toxin A-induced murine ileal enteritis. *Infect*
856 *Immun* **74**, 2606-2612 (2006).
857
858 58. Ma N, Zhang J, Reiter RJ, Ma X. Melatonin mediates mucosal immune
859 cells, microbial metabolism, and rhythm crosstalk: A therapeutic target
860 to reduce intestinal inflammation. *Med Res Rev* **40**, 606-632 (2020).
861
862 59. Yang G*, et al.* Expression of recombinant Clostridium difficile toxin A and
863 B in Bacillus megaterium. *BMC Microbiol* **8**, 192 (2008).
864
865 60. Reeves AE, Theriot CM, Bergin IL, Huffnagle GB, Schloss PD, Young
866 VB. The interplay between microbiome dynamics and pathogen
867 dynamics in a murine model of Clostridium difficile Infection. *Gut*

868 *Microbes* **2**, 145-158 (2011).
869

870

871

872 **Figures**

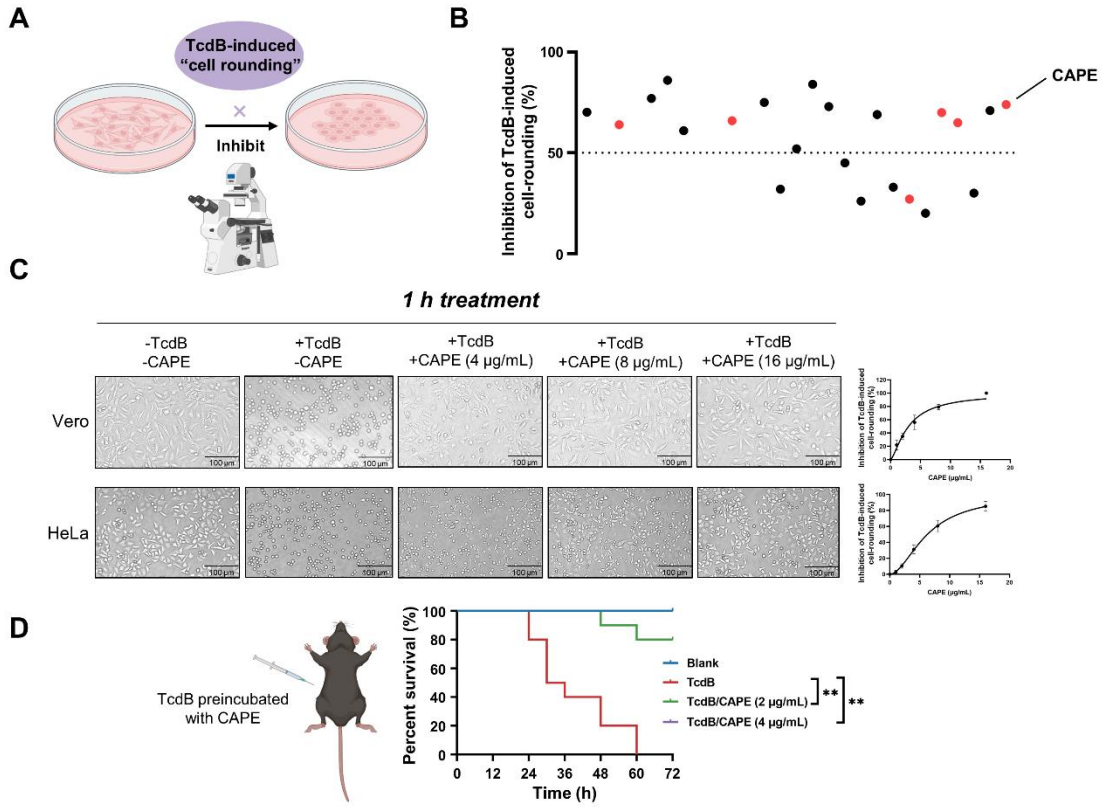

873

874 **Figure 1. CAPE suppresses TcdB-mediated cell rounding.**

875 **(A)** Schematic of the process used for the identification of small molecules that
876 inhibit the cell rounding phenotype induced by TcdB. TcdB (0.2 ng/mL) was
877 preincubated with 8 μg/mL of individual compounds prior to addition to the cell
878 cultures. **(B)** Active compounds were identified from the chemical library
879 consisting of 2076 chemicals. The red dots represent caffeic acid and its
880 derivatives. **(C)** Dose-dependent CAPE inhibition of TcdB-induced rounding of
881 Vero (upper) and HeLa (lower) cells. Scale bar, 100 μm. The dose titration
882 curves are presented on the right. **(D)** The survival rates of mice that were
883 intraperitoneally injected with CAPE-pretreated or native TcdB (30 ng). * p <0.05
884 and ** p <0.01 by log-rank (Mantel–Cox) test.

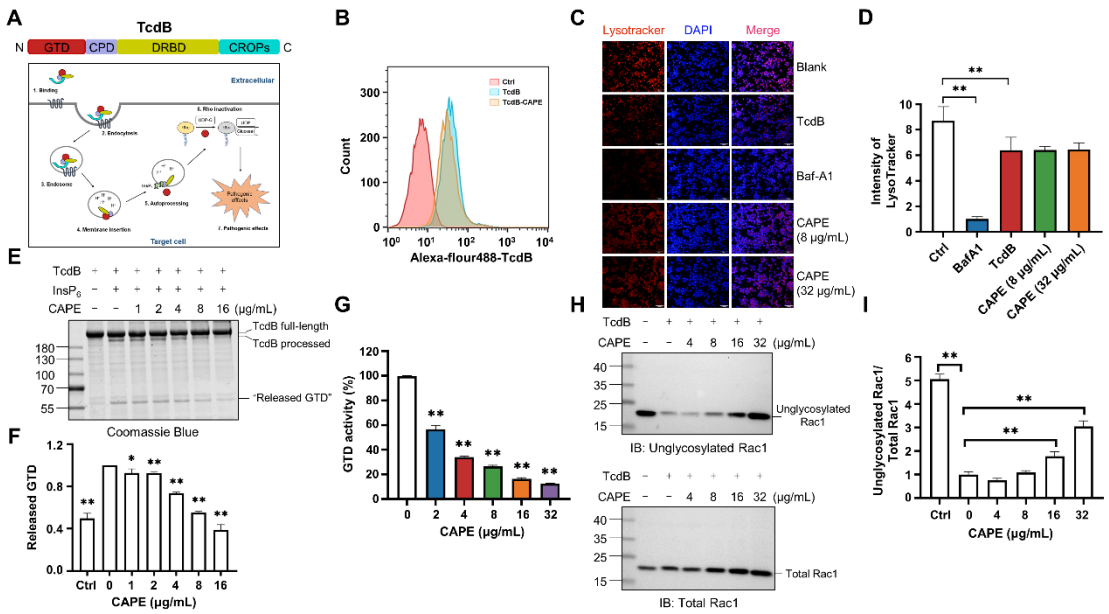

885

886 **Figure 2. Mechanism by which CAPE suppresses TcdB intoxication.**

887 **(A)** Schematic illustration of the multistep mechanism of TcdB intoxication of
888 host cells. **(B)** Determination of internalized TcdB levels. Alexa Fluor 488-
889 labeled TcdB was incubated with 32 μg/mL CAPE for 30 min before it was
890 added to the cell culture. The cellular uptake of TcdB was measured by flow
891 cytometry analysis. **(C)** Lysosomal activity in host cells treated with CAPE was
892 measured via LysoTracker staining. The nuclei were stained with DAPI. Bar,
893 100 μm. **(D)** The intensities of LysoTracker staining were quantified using
894 ImageJ. * p <0.05; ** p <0.01 using one-way ANOVA. **(E-F)** CAPE inhibits $InsP_6$-
895 induced autoprocessing of full-length TcdB. Two micrograms of TcdB was
896 preincubated with increasing concentrations of CAPE for 1 h. Self-cleavage of
897 TcdB was initiated by the addition of 3 μg of $InsP_6$ and the cells were incubated
898 for 6 h at 37 °C. Reactions were terminated with 5x SDS loading buffer, and the
899 release of GTD was visualized by CBB staining of the SDS–PAGE gel **(E)**. The
900 level of released GTD in panel E was quantified by ImageJ **(F)** * p <0.05; ** p

901 <0.01 using one-way ANOVA. **(G)** Dose-dependent inhibition of the GTD
902 activity of TcdB by CAPE. Recombinant GTD of TcdB was mixed with different
903 concentrations of CAPE (0-32 μg/mL) and incubated for 15 min at 25 ºC. GTD
904 activity was measured by the UDP-Glo™ glycosyltransferase assay. **(H-I)**
905 Intracellular Rac1 glucosylation in cells treated with TcdB. Native or CAPE-
906 pretreated TcdB was added to the cell culture and cells were incubated for 2 h.
907 The cells were lysed, and the glucosylation of Rac1 was analyzed by western
908 blotting using antibodies recognizing total Rac1 and unglycosylated Rac1 **(H)**.
909 The level of Rac1 glucosylation shown in H was quantified by ImageJ **(I)**. * *p*
910 <0.05; ** *p* <0.01 using one-way ANOVA.
911

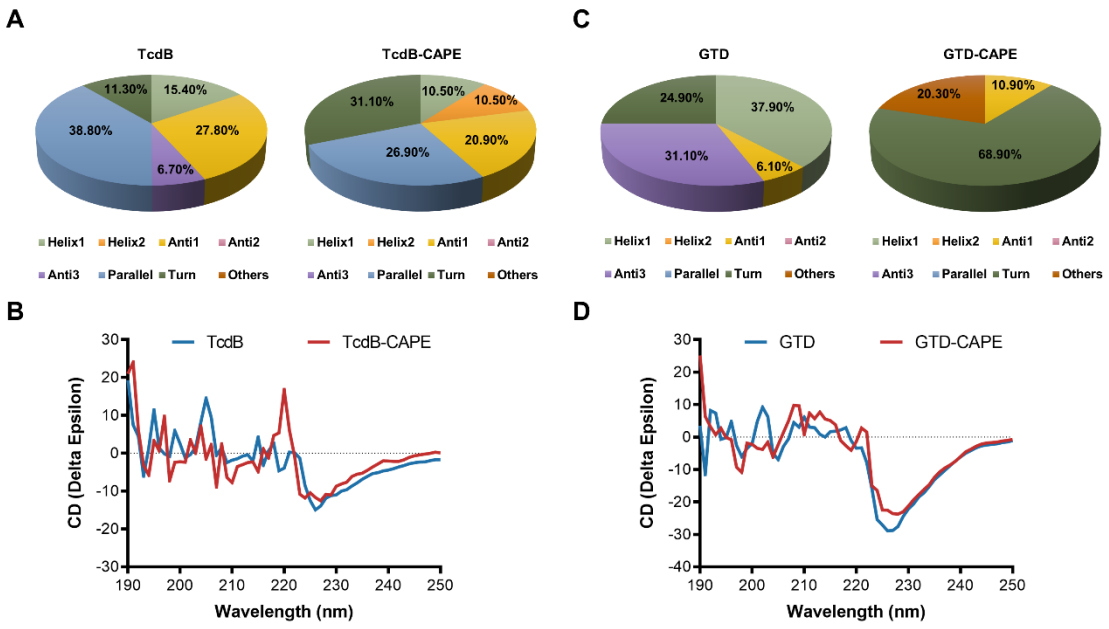

Figure 3. CAPE alters the secondary structure of TcdB and GTD.

(A-B) The secondary structure of TcdB **(A)** or GTD **(B)** in the presence or absence of 32 μg/mL CAPE was determined by CD spectroscopy. **(C-D)** Calculated CD spectra of CAPE-treated TcdB **(C)** and GTD **(D)**. The wavelength for CD spectroscopy was set at 190-250 nm.

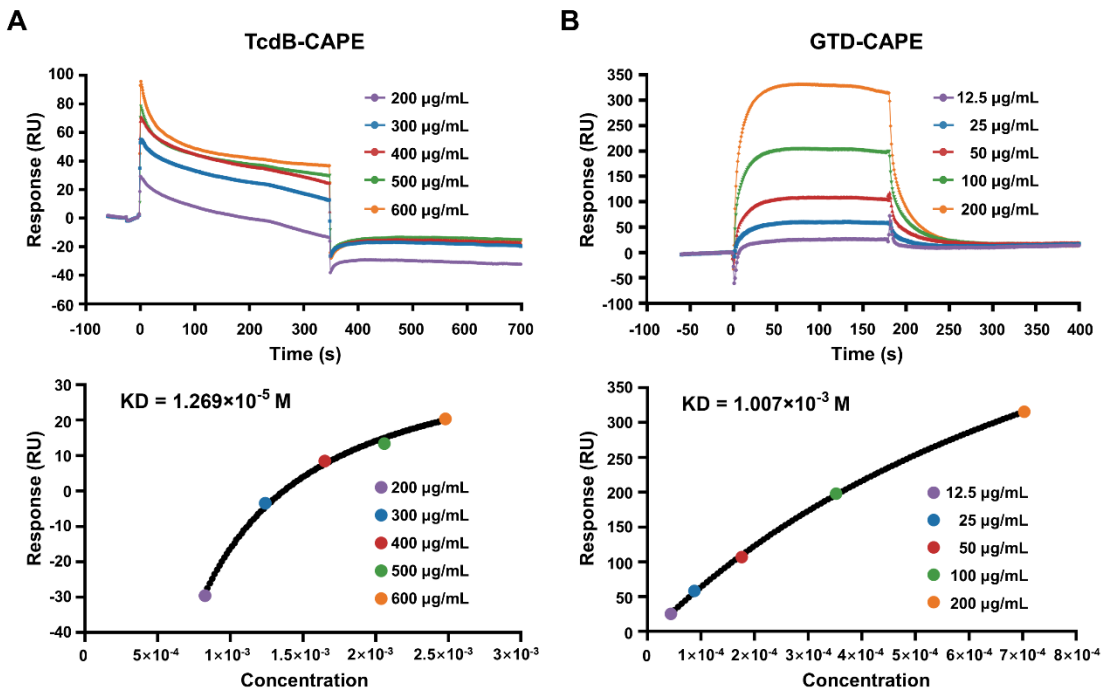

Figure 4. Direct interaction of CAPE with TcdB and GTD.

(A-B) Full-length TcdB or GTD was immobilized on a CM5 chip, followed by the injection of various concentrations of CAPE. The response unit (RU) value and affinities of CAPE interactions with TcdB **(A)** and GTD **(B)** were determined by a Biacore T100.

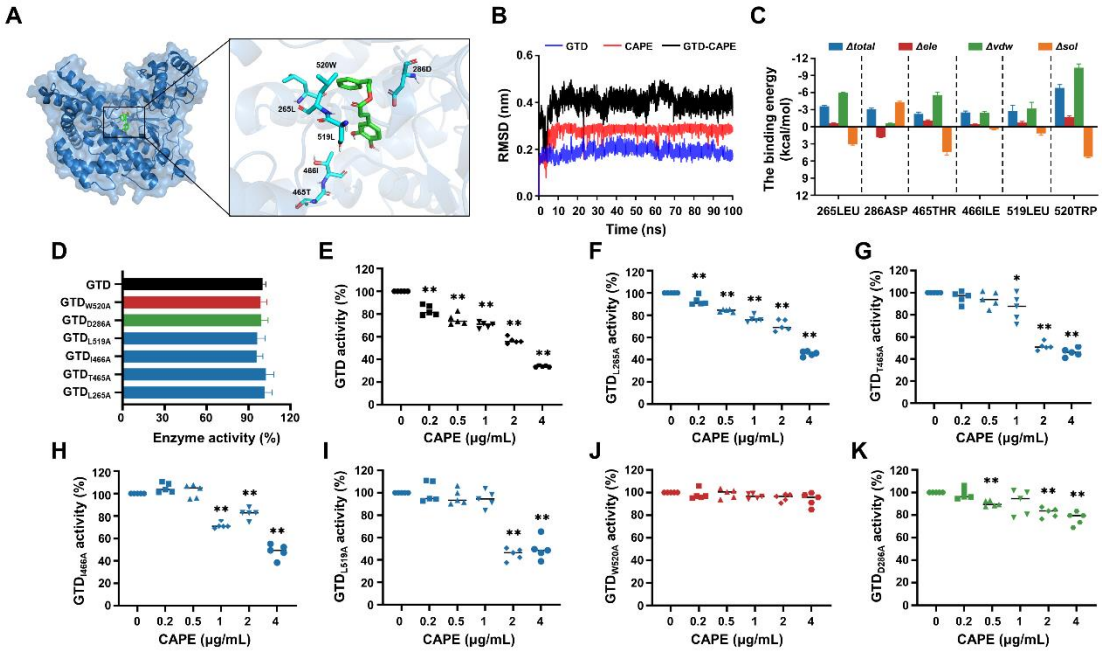

Figure 5. Asp286 and Trp520 in the GTD are critical for CAPE-mediated inhibition of GTD.

(A) Three-dimensional structure determination of GTD with the CAPE complex was performed by molecular modeling. **(B)** The RMSD values of the GTD-CAPE complex. **(C)** Decomposition of the binding energy on a per-residue basis in the binding sites of the GTD-CAPE complex. **(D)** Glucosyltransferase activity of wild-type GTD and the GTD mutants. **(E-K)** Residual activity of wild-type GTD **(E)** and its mutants GTD_{L265A} **(F)**, GTD_{T465A} **(G)**, GTD_{I466A} **(H)**, GTD_{L519A} **(I)**, GTD_{W520A} **(J)** and GTD_{D286A} **(K)** in the presence of increasing concentrations of CAPE (0-4 μg/mL). * p <0.05; ** p <0.01 using one-way ANOVA.

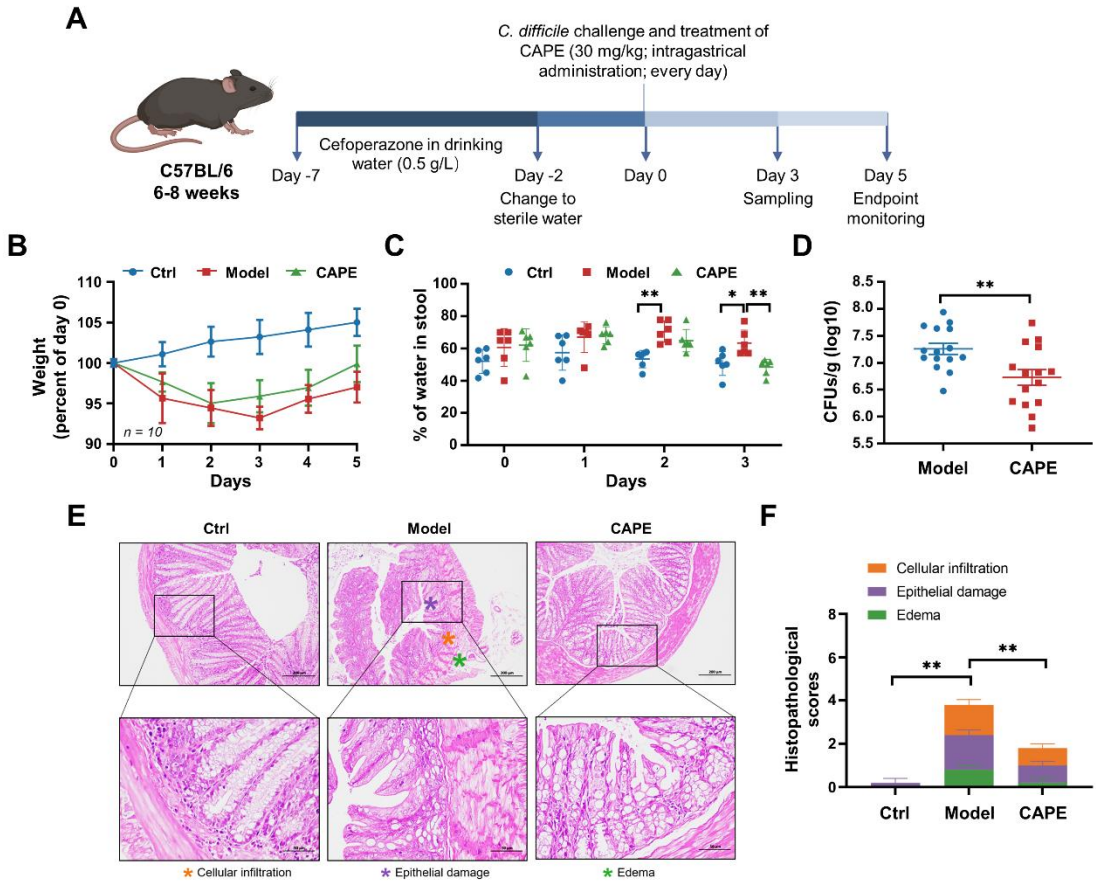

Figure 6. CAPE treatment blocks the pathology of CDI in mice.

(A) Schematic of the process used for the establishment of the CDI mouse model. **(B)** Weight changes in CDI mice after CAPE or vehicle treatment (n=10). **(C)** The fecal dry/wet weight ratio in CDI mice treated with CAPE or vehicle (n=6). * p <0.05; ** p <0.01 using one-way ANOVA. **(D)** Bacterial colonization in the feces of CDI mice treated with CAPE or vehicle (n=15). * p <0.05; ** p <0.01 using the Mann–Whitney U test. **(E)** Pathological analysis of colon sections from CDI mice treated with CAPE or vehicle. The black boxes are the regions that were magnified and are shown underneath. **(F)** Histopathological scores of vehicle-treated and CAPE-treated mice in terms of cell infiltration (orange), epithelial damage (purple), and edema (green). * p <0.05; ** p <0.01

using one-way ANOVA.

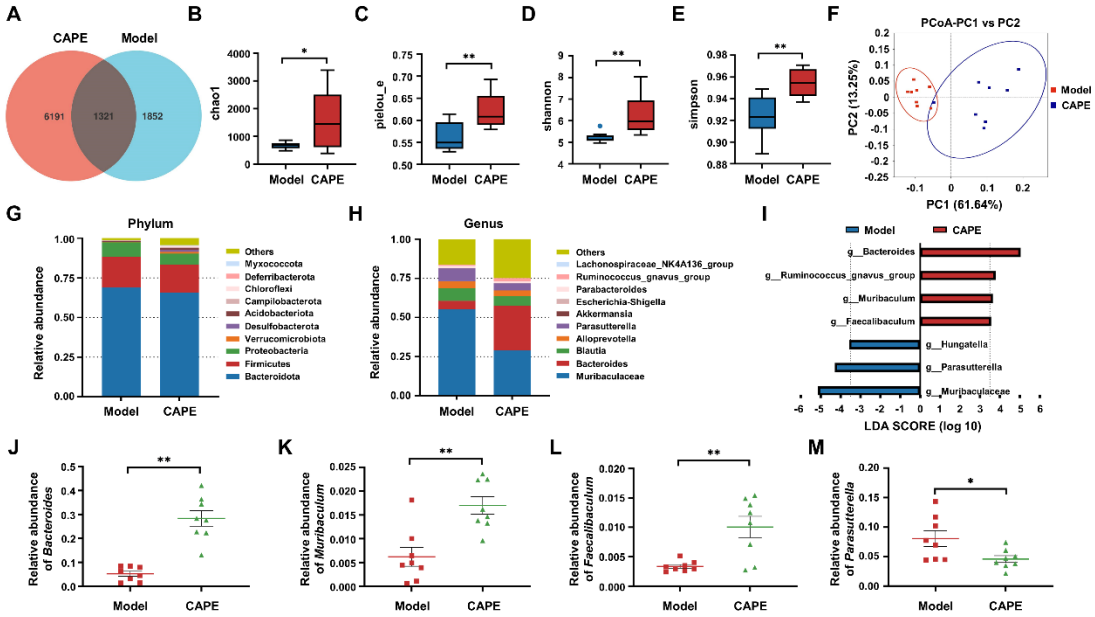

Figure 7. The influence of CAPE treatment on the diversity and composition of the gut microbiota in CDI mice.

(A) Venn diagram illustrating the numbers of differentially abundant bacteria identified using a single model and their cooperation. **(B-E)** Quantification of the α diversity of the gut microbiota according to the observed species richness **(B-C),** Shannon index **(D)**, and Simpson index **(E)**. **(F)** PCoA showing β diversity based on the weighted UniFrac distance. **(G-H)** Relative abundance of the top 10 predominant bacteria classified at the phylum **(G)** and genus **(H)** levels. **(I)** Significant changes in flora among the model and CAPE groups, as measured by LEfSe analysis (LDA score [log 10] > 3.5). **(J-M)** Relative abundances of *Bacteroides* **(J)**, *Muribaculum* **(K)**, *Faecalibaculum* **(L)**, and *Parasutterella* **(M)** in mice in the model and CAPE treatment groups. * p <0.05; ** p <0.01 using an unpaired Student's t test.

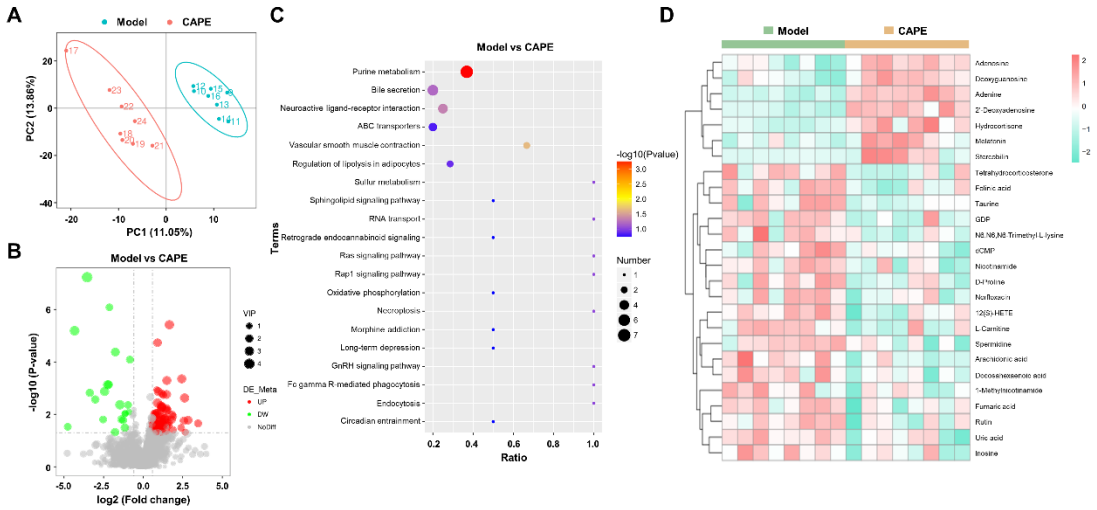

Figure 8. Alterations in gut metabolites in CAPE-treated mice with CDI. **(A)** The score plots show orthogonal partial least square discriminant analysis (PLS-DA) results. **(B)** Volcano plot representing the upregulated or downregulated gut metabolites in the CAPE treatment group compared to those in the model group. **(C)** Enrichment bubble map of the top 20 metabolic pathways in the CAPE treatment and model groups. **(D)** The 26 potential biomarkers are displayed in a heatmap, along with hierarchical clustering analysis.

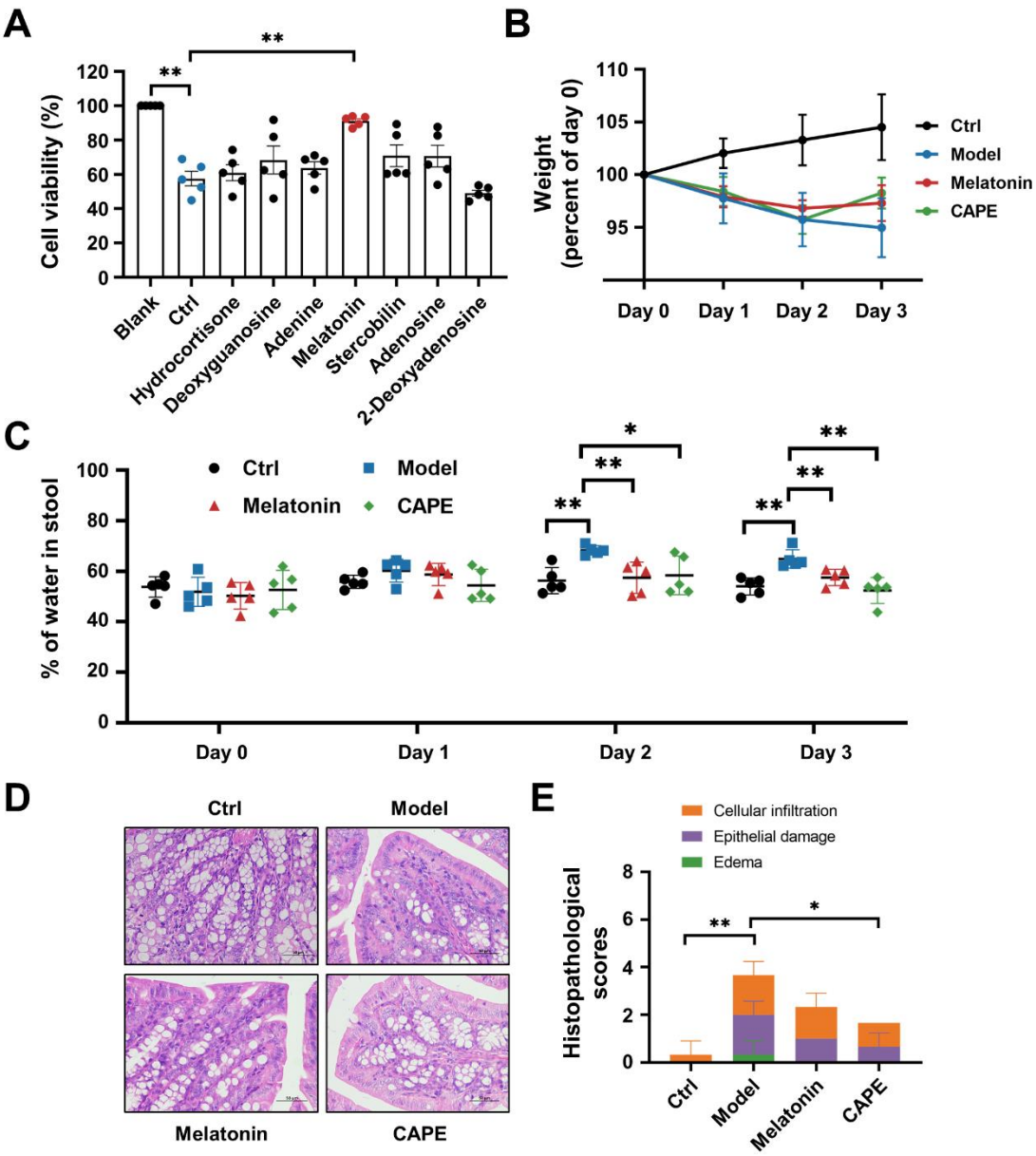

Figure 9. Oral administration of melatonin alleviates the pathology of CDI. **(A)** The impact of upregulated metabolites on the cytotoxicity of TcdB. TcdB (0.2 ng/mL) was incubated with each of the metabolites (100 μg/mL) for 1 h at 37 ºC before being added to the Vero cell culture. At 3 h after TcdB treatment, cell death was evaluated with a CCK-8 kit. **(B)** Body weight changes in melatonin-treated CDI mice (n=5). **(C)** The fecal dry/wet weight ratio in CDI mice after melatonin treatment (n=5). **(D)** Histopathological analysis of colon tissue from

982 CDI mice treated with melatonin. **(E)** Histopathological scores of melatonin-

983 treated CDI mice. * $p < 0.05$; ** $p < 0.01$ using one-way ANOVA.

984

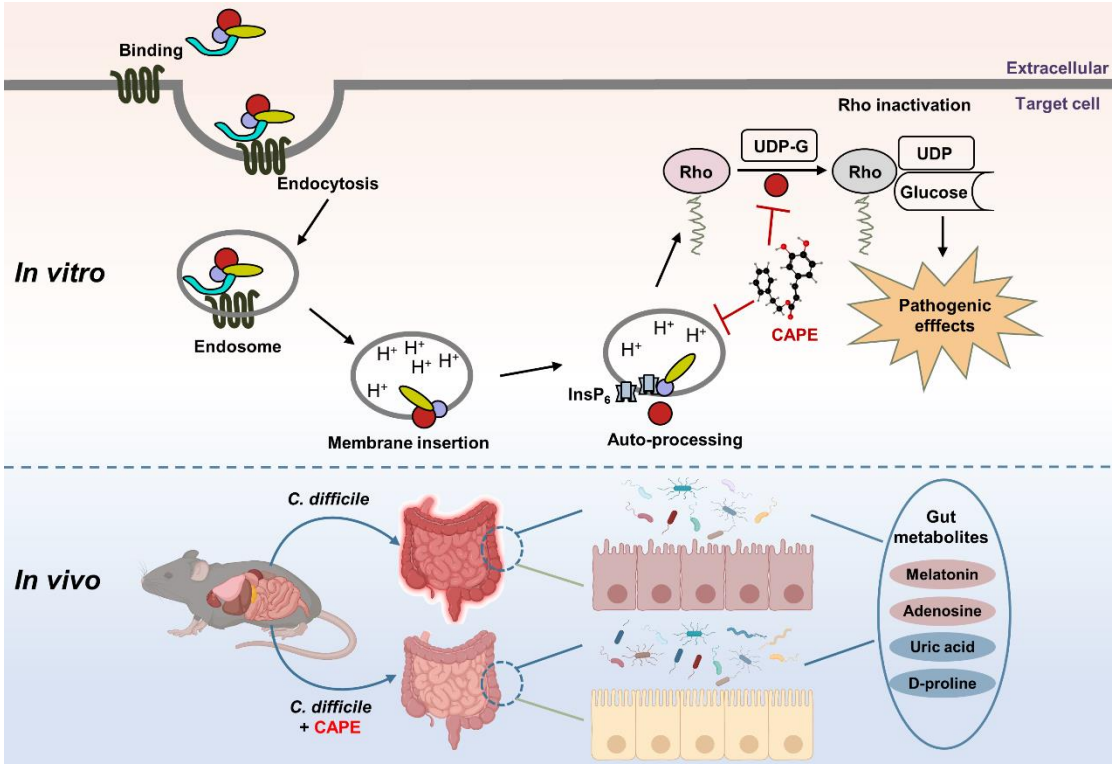

Figure 10. A model for CAPE-mediated suppression of TcdB cytotoxicity and protection of mice from CDI.

The intoxication of cells by TcdB involves multistep mechanisms. Direct interaction of CAPE with full-length TcdB blocks $InsP_6$-induced autoproteolysis, resulting in decreased production of active GTD. The binding between GTD and CAPE inhibits its glucosyltransferase activity, thus decreasing the glucosylation level of Rac1. CAPE treatment of CDI mice markedly restored the diversity and composition of the gut microbiota and induced changes in gut metabolites, which might have contributed to the therapeutic outcomes of CDI following CAPE treatment.

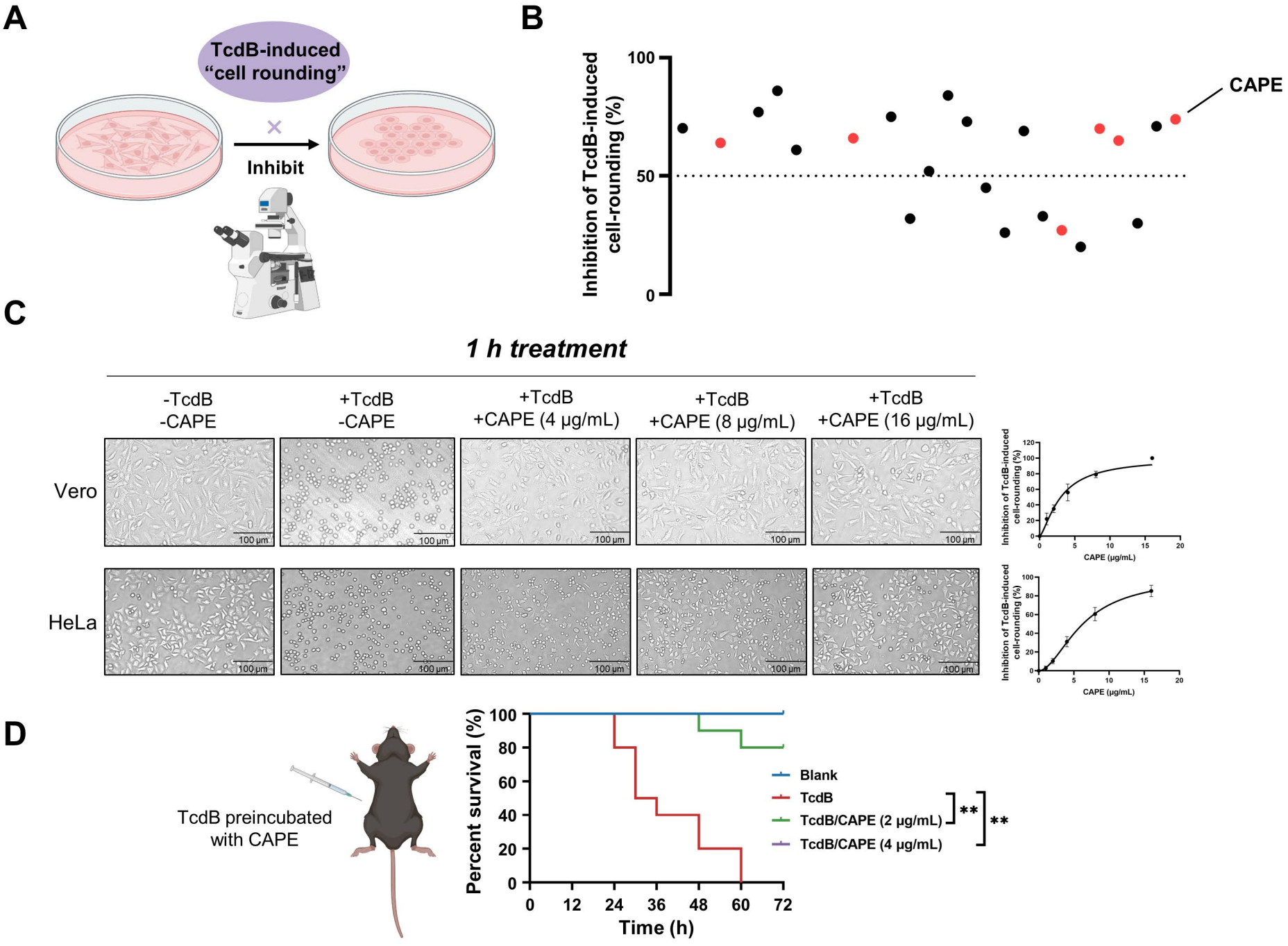
A
TcdB-induced
"cell rounding"
Inhibit
B
Inhibition of TcdB-induced cell-rounding (%)
100
50
0
CAPE
C
1 h treatment
-TcdB
-CAPE
+TcdB
-CAPE
+TcdB
+CAPE (4 μg/mL)
+TcdB
+CAPE (8 μg/mL)
+TcdB
+CAPE (16 μg/mL)
Vero
HeLa
100 μm
Inhibition of TcdB-induced cell-rounding (%)
CAPE (μg/mL)
D
TcdB preincubated
with CAPE
Percent survival (%)
Time (h)
Blank
TcdB
TcdB/CAPE (2 μg/mL)
TcdB/CAPE (4 μg/mL)
**
**

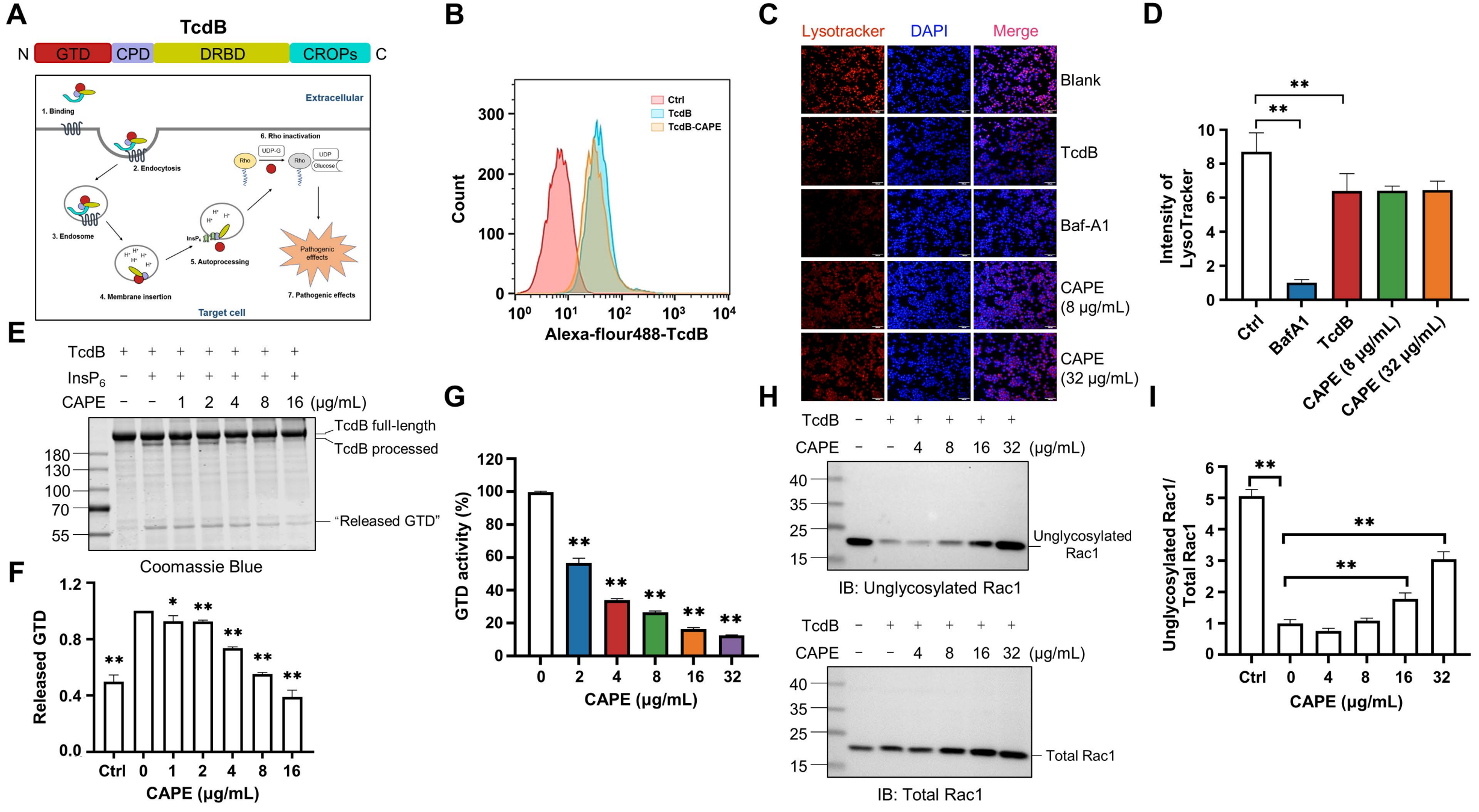
A
TcdB
N
GTD
CPD
DRBD
CROPs
C
Extracellular
1. Binding
2. Endocytosis
3. Endosome
4. Membrane insertion
5. Autoprocessing
6. Rho inactivation
UDP-G
UDP
Glucose
Rho
Pathogenic effects
7. Pathogenic effects
Target cell
B
Ctrl
TcdB
TcdB-CAPE
Count
Alexa-flour488-TcdB
C
Lysotracker
DAPI
Merge
Blank
TcdB
Baf-A1
CAPE (8 μg/mL)
CAPE (32 μg/mL)
D
Intensity of LysoTracker
Ctrl
BafA1
TcdB
CAPE (8 μg/mL)
CAPE (32 μg/mL)
E
TcdB
InsP6
CAPE (μg/mL)
TcdB full-length
TcdB processed
"Released GTD"
Coomassie Blue
F
Released GTD
CAPE (μg/mL)
G
GTD activity (%)
CAPE (μg/mL)
H
TcdB
CAPE (μg/mL)
Unglycosylated Rac1
IB: Unglycosylated Rac1
Total Rac1
IB: Total Rac1
I
Unglycosylated Rac1/ Total Rac1
CAPE (μg/mL)

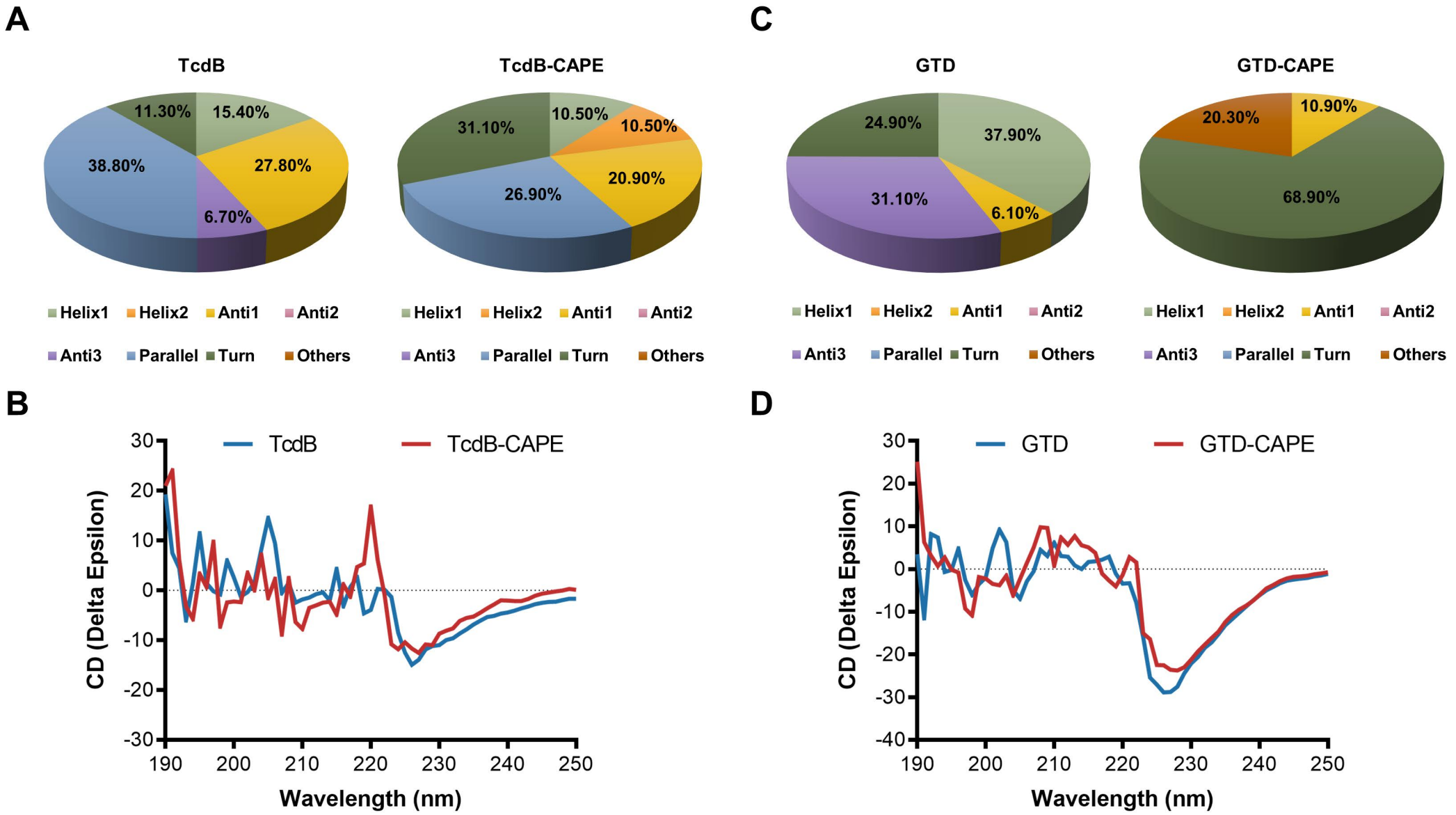
A
TcdB
11.30%
15.40%
38.80%
27.80%
6.70%
TcdB-CAPE
31.10%
10.50%
10.50%
20.90%
26.90%
Helix1
Helix2
Anti1
Anti2
Anti3
Parallel
Turn
Others
C
GTD
24.90%
37.90%
31.10%
6.10%
GTD-CAPE
20.30%
10.90%
68.90%
B
TcdB
TcdB-CAPE
CD (Delta Epsilon)
Wavelength (nm)
D
GTD
GTD-CAPE
CD (Delta Epsilon)
Wavelength (nm)

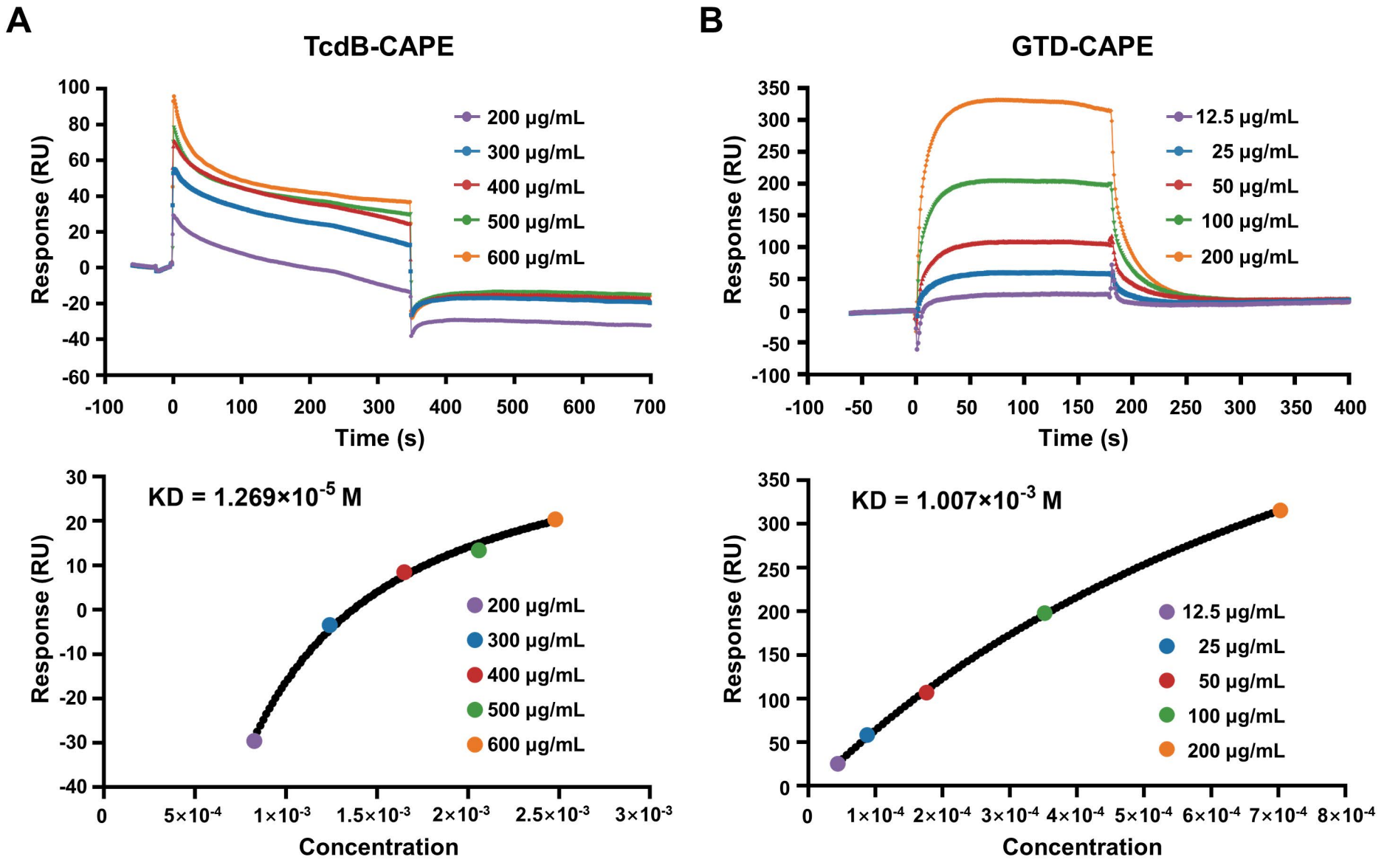
A
TcdB-CAPE
Response (RU)
Time (s)
200 μg/mL
300 μg/mL
400 μg/mL
500 μg/mL
600 μg/mL
KD = 1.269×10-5 M
Concentration
B
GTD-CAPE
Response (RU)
Time (s)
12.5 μg/mL
25 μg/mL
50 μg/mL
100 μg/mL
200 μg/mL
KD = 1.007×10-3 M
Concentration

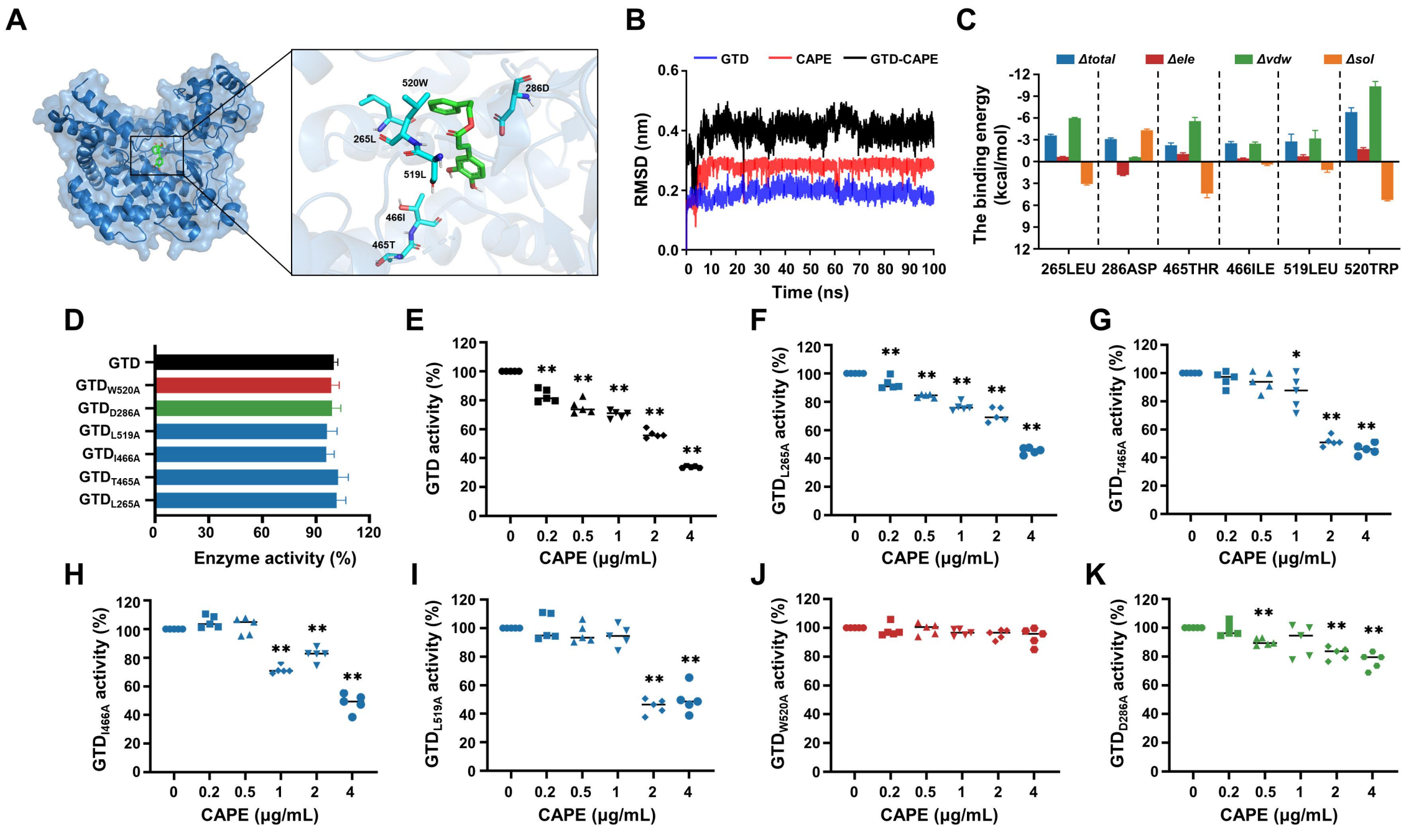
A
520W
286D
265L
519L
466I
465T
B
GTD
CAPE
GTD-CAPE
RMSD (nm)
Time (ns)
C
Δtotal
Δele
Δvdw
Δsol
The binding energy (kcal/mol)
265LEU
286ASP
465THR
466ILE
519LEU
520TRP
D
GTD
GTD$_{W520A}$
GTD$_{D286A}$
GTD$_{L519A}$
GTD$_{I466A}$
GTD$_{T465A}$
GTD$_{L265A}$
Enzyme activity (%)
E
GTD activity (%)
CAPE (μg/mL)
F
GTD$_{L265A}$ activity (%)
G
GTD$_{T465A}$ activity (%)
H
GTD$_{I466A}$ activity (%)
I
GTD$_{L519A}$ activity (%)
J
GTD$_{W520A}$ activity (%)
K
GTD$_{D286A}$ activity (%)

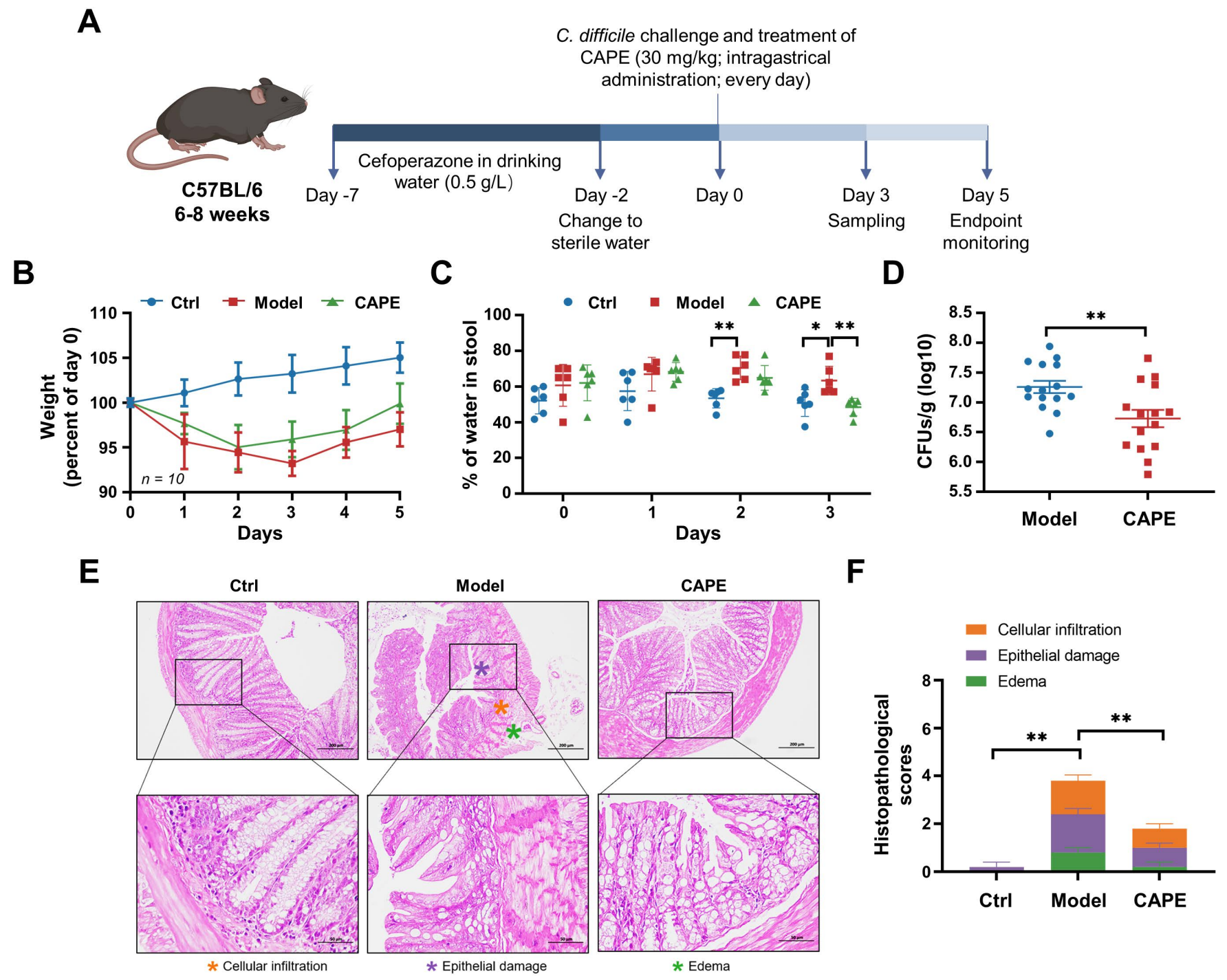
A
C. difficile challenge and treatment of CAPE (30 mg/kg; intragastrical administration; every day)
C57BL/6
6-8 weeks
Cefoperazone in drinking water (0.5 g/L)
Day -7
Day -2
Change to sterile water
Day 0
Day 3
Sampling
Day 5
Endpoint monitoring
B
Ctrl
Model
CAPE
Weight (percent of day 0)
n = 10
Days
C
% of water in stool
Days
D
CFUs/g (log10)
Model
CAPE
E
Ctrl
Model
CAPE
Cellular infiltration
Epithelial damage
Edema
F
Cellular infiltration
Epithelial damage
Edema
Histopathological scores
Ctrl
Model
CAPE

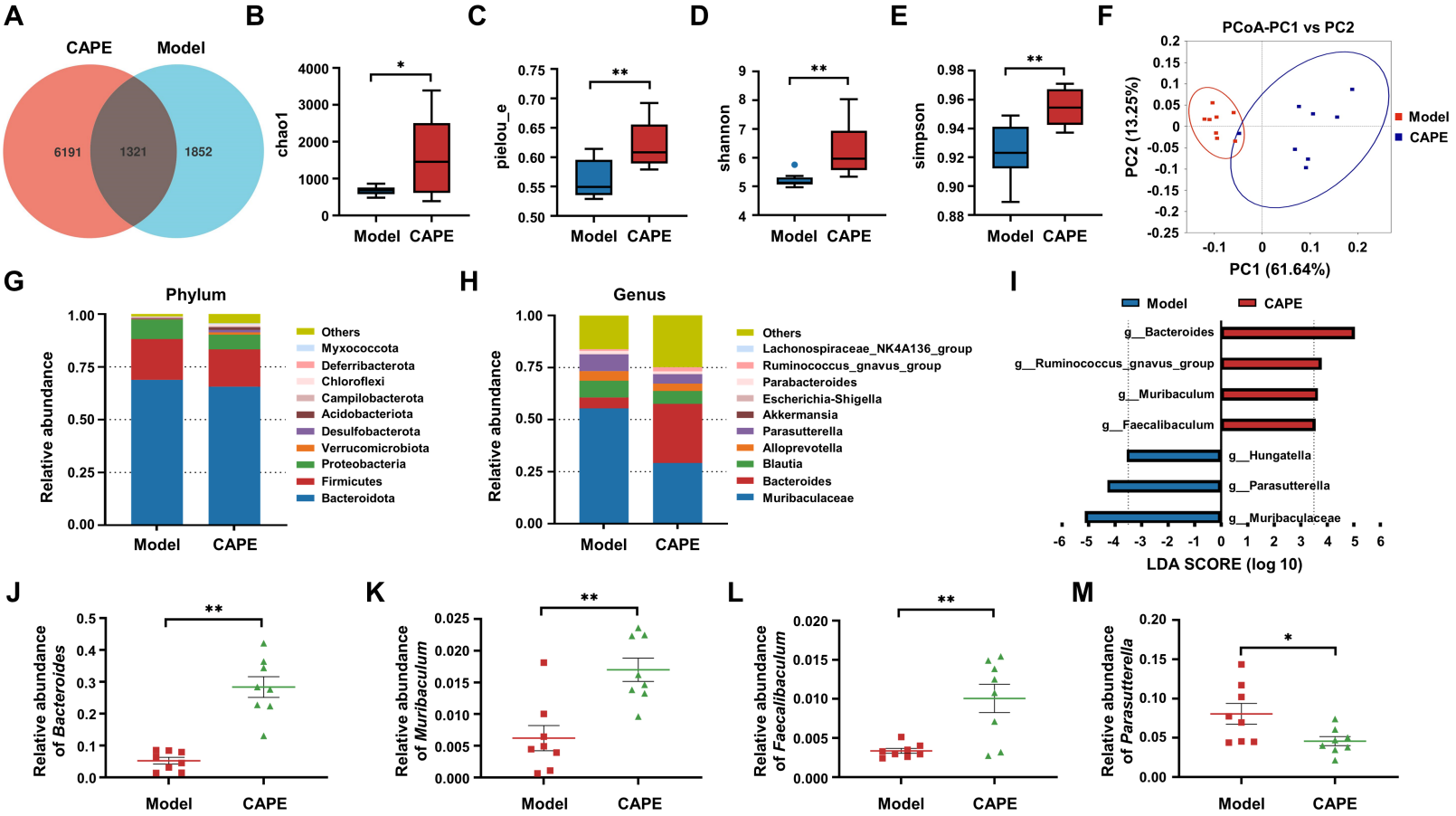
A
CAPE
Model
6191
1321
1852
B
chao1
Model
CAPE
C
pielou_e
D
shannon
E
simpson
F
PCoA-PC1 vs PC2
PC2 (13.25%)
PC1 (61.64%)
Model
CAPE
G
Phylum
Relative abundance
Others
Myxococcota
Deferribacterota
Chloroflexi
Campilobacterota
Acidobacteriota
Desulfobacterota
Verrucomicrobiota
Proteobacteria
Firmicutes
Bacteroidota
H
Genus
Others
Lachonospiraceae_NK4A136_group
Ruminococcus_gnavus_group
Parabacteroides
Escherichia-Shigella
Akkermansia
Parasutterella
Alloprevotella
Blautia
Bacteroides
Muribaculaceae
I
g__Bacteroides
g__Ruminococcus_gnavus_group
g__Muribaculum
g__Faecalibaculum
g__Hungatella
g__Parasutterella
g__Muribaculaceae
LDA SCORE (log 10)
J
Relative abundance of Bacteroides
K
Relative abundance of Muribaculum
L
Relative abundance of Faecalibaculum
M
Relative abundance of Parasutterella

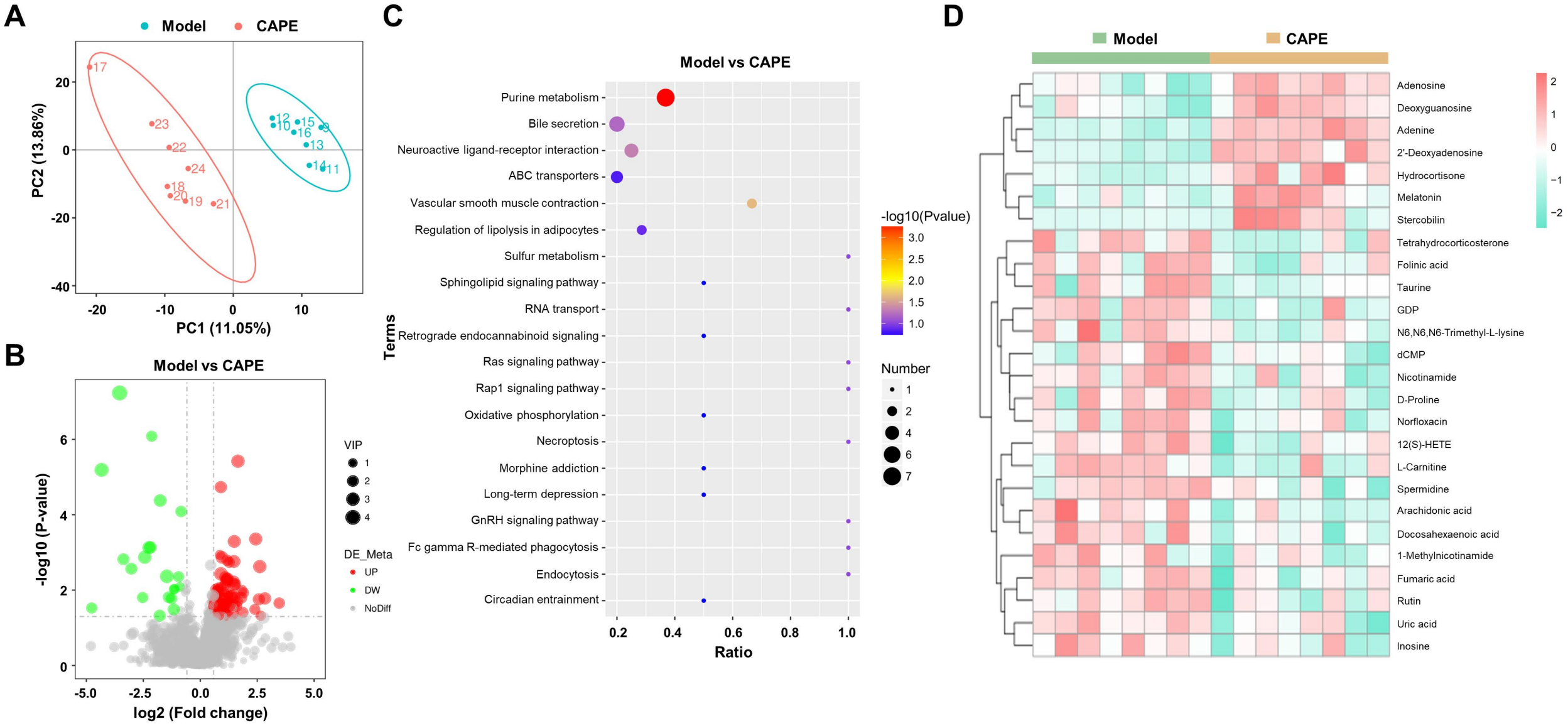
A
Model
CAPE
PC2 (13.86%)
PC1 (11.05%)
B
Model vs CAPE
-log10 (P-value)
log2 (Fold change)
VIP
DE_Meta
UP
DW
NoDiff
C
Model vs CAPE
Purine metabolism
Bile secretion
Neuroactive ligand-receptor interaction
ABC transporters
Vascular smooth muscle contraction
Regulation of lipolysis in adipocytes
Sulfur metabolism
Sphingolipid signaling pathway
RNA transport
Retrograde endocannabinoid signaling
Ras signaling pathway
Rap1 signaling pathway
Oxidative phosphorylation
Necroptosis
Morphine addiction
Long-term depression
GnRH signaling pathway
Fc gamma R-mediated phagocytosis
Endocytosis
Circadian entrainment
Terms
Ratio
-log10(Pvalue)
Number
D
Model
CAPE
Adenosine
Deoxyguanosine
Adenine
2'-Deoxyadenosine
Hydrocortisone
Melatonin
Stercobilin
Tetrahydrocorticosterone
Folinic acid
Taurine
GDP
N6,N6,N6-Trimethyl-L-lysine
dCMP
Nicotinamide
D-Proline
Norfloxacin
12(S)-HETE
L-Carnitine
Spermidine
Arachidonic acid
Docosahexaenoic acid
1-Methylnicotinamide
Fumaric acid
Rutin
Uric acid
Inosine

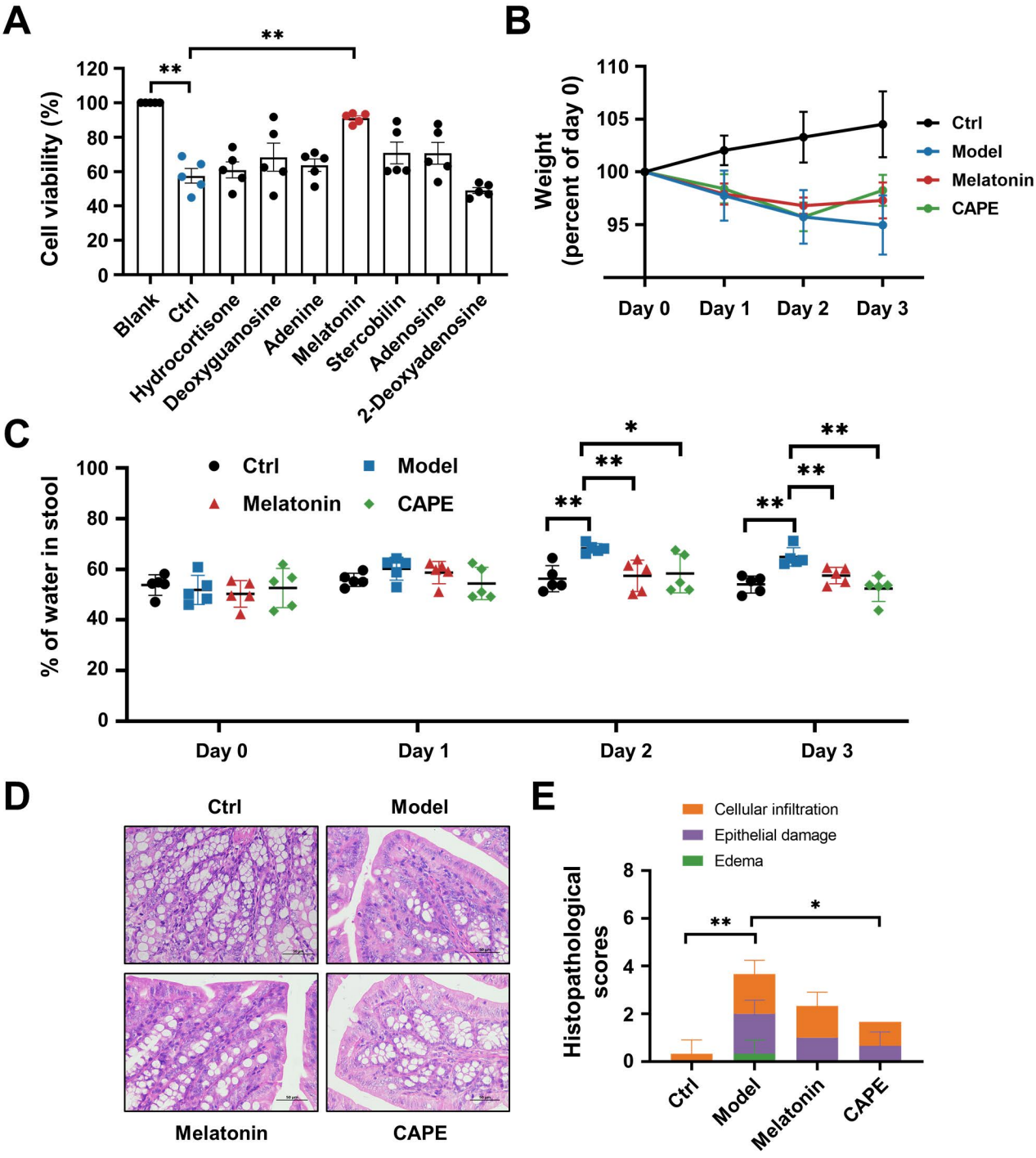
A
Cell viability (%)
120
100
80
60
40
20
0
**
**
Blank
Ctrl
Hydrocortisone
Deoxyguanosine
Adenine
Melatonin
Stercobilin
Adenosine
2-Deoxyadenosine
B
Weight (percent of day 0)
110
105
100
95
Day 0
Day 1
Day 2
Day 3
Ctrl
Model
Melatonin
CAPE
C
% of water in stool
100
80
60
40
20
0
Ctrl
Model
Melatonin
CAPE
*
**
**
**
**
**
Day 0
Day 1
Day 2
Day 3
D
Ctrl
Model
Melatonin
CAPE
E
Histopathological scores
Cellular infiltration
Epithelial damage
Edema
8
6
4
2
0
**
*
Ctrl
Model
Melatonin
CAPE

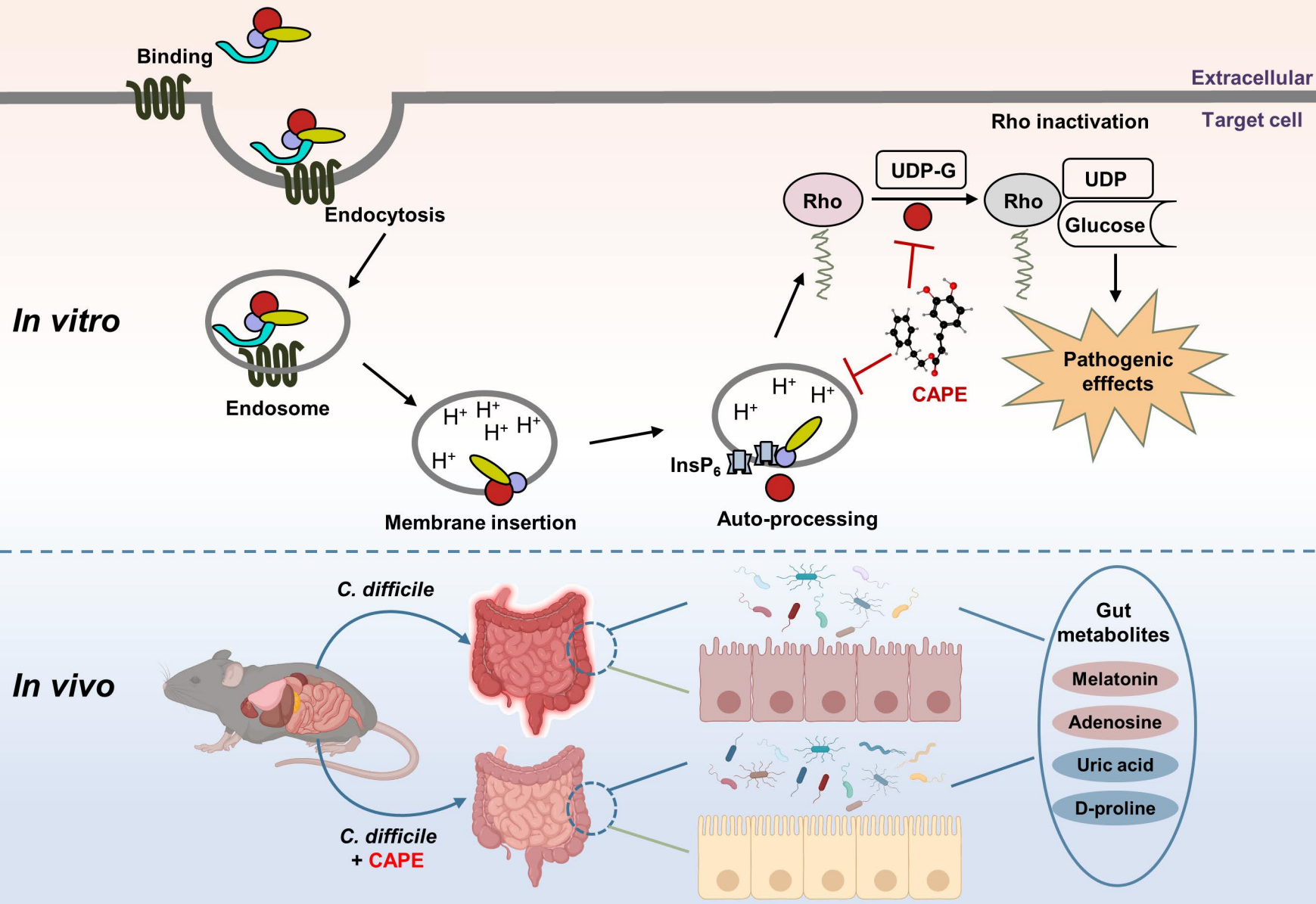
Binding
Extracellular
Target cell
Endocytosis
Rho inactivation
UDP-G
Rho
Rho
UDP
Glucose
In vitro
Endosome
H+
Membrane insertion
InsP6
Auto-processing
CAPE
Pathogenic
efffects
In vivo
C. difficile
C. difficile
+ CAPE
Gut
metabolites
Melatonin
Adenosine
Uric acid
D-proline

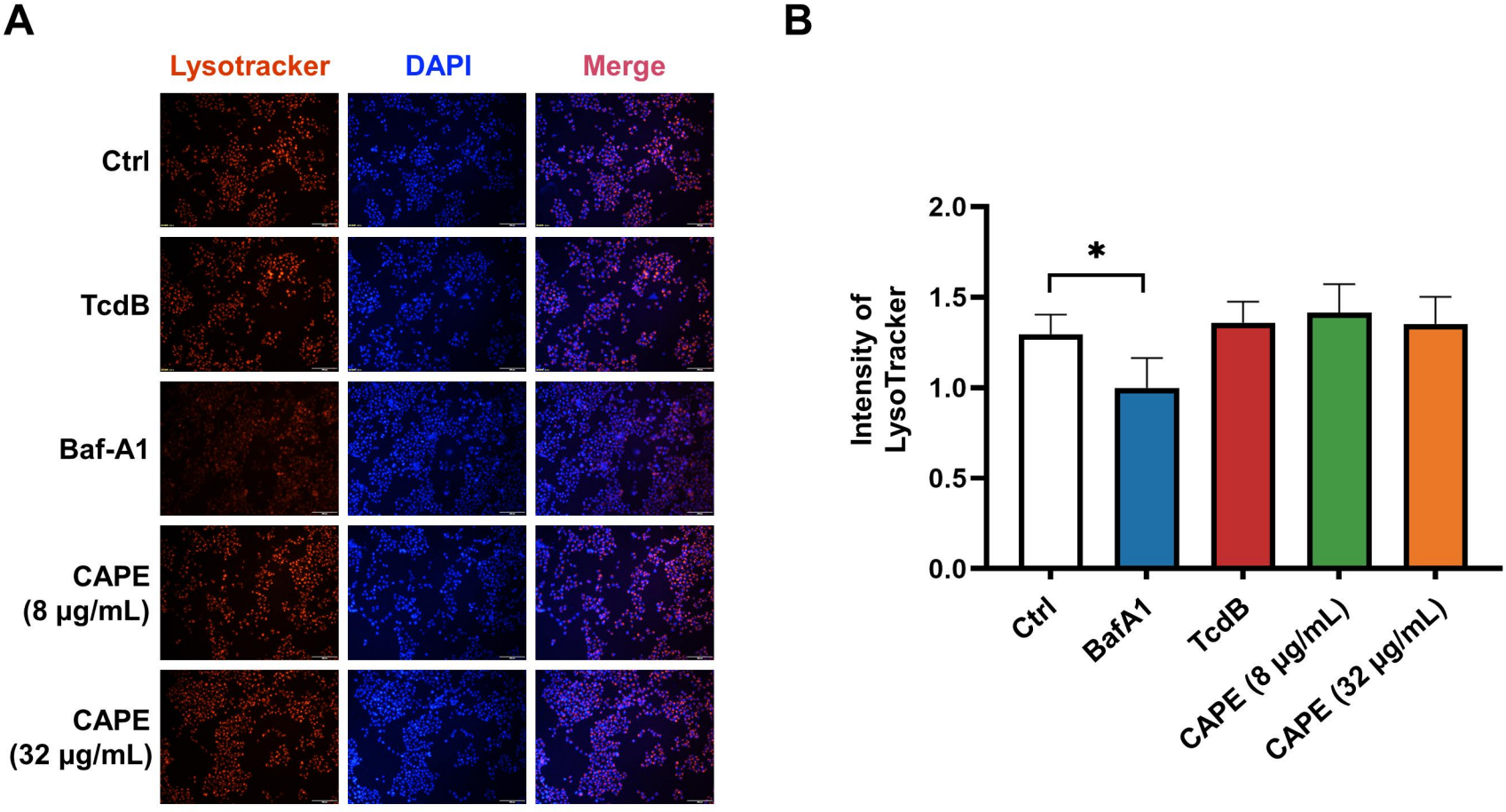
A
Lysotracker
DAPI
Merge
Ctrl
TcdB
Baf-A1
CAPE
(8 μg/mL)
CAPE
(32 μg/mL)
B
Intensity of
LysoTracker
2.0
1.5
1.0
0.5
0.0
*
Ctrl
BafA1
TcdB
CAPE (8 μg/mL)
CAPE (32 μg/mL)

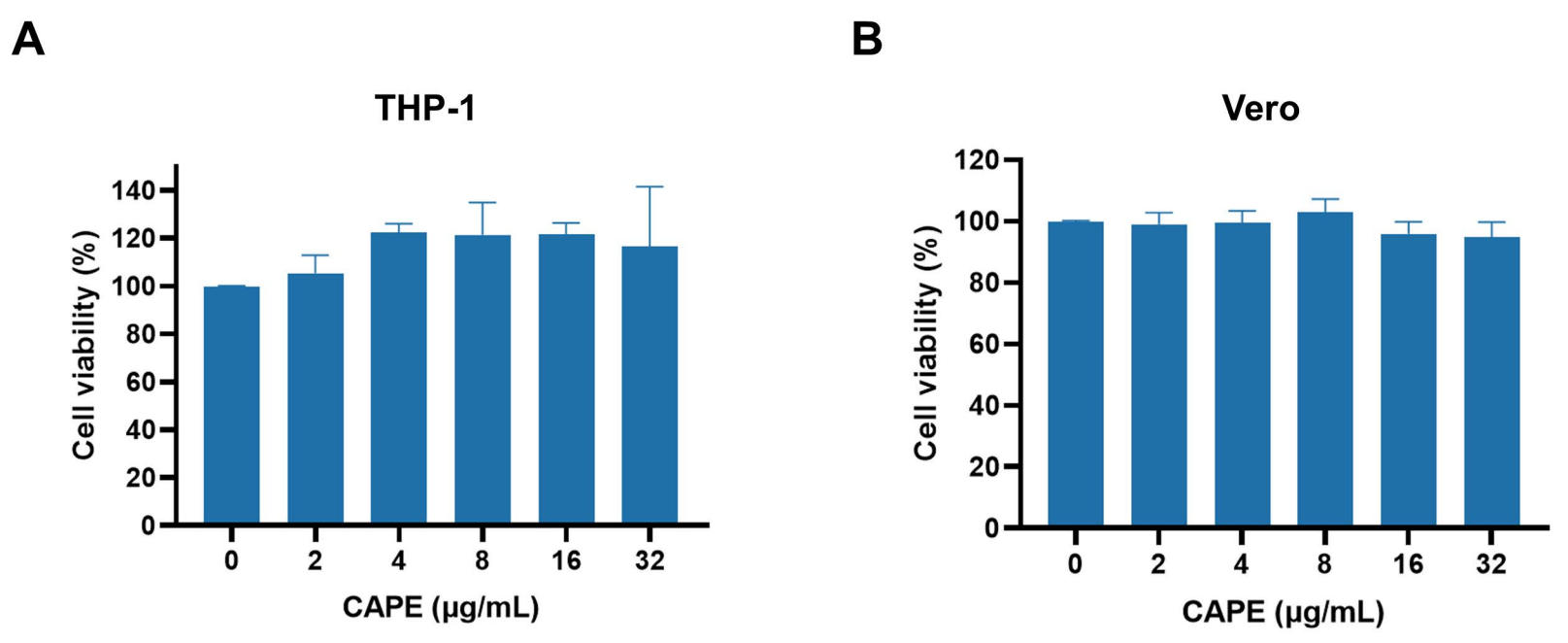
A
THP-1
Cell viability (%)
140
120
100
80
60
40
20
0
0
2
4
8
16
32
CAPE (μg/mL)
B
Vero
Cell viability (%)
120
100
80
60
40
20
0
0
2
4
8
16
32
CAPE (μg/mL)

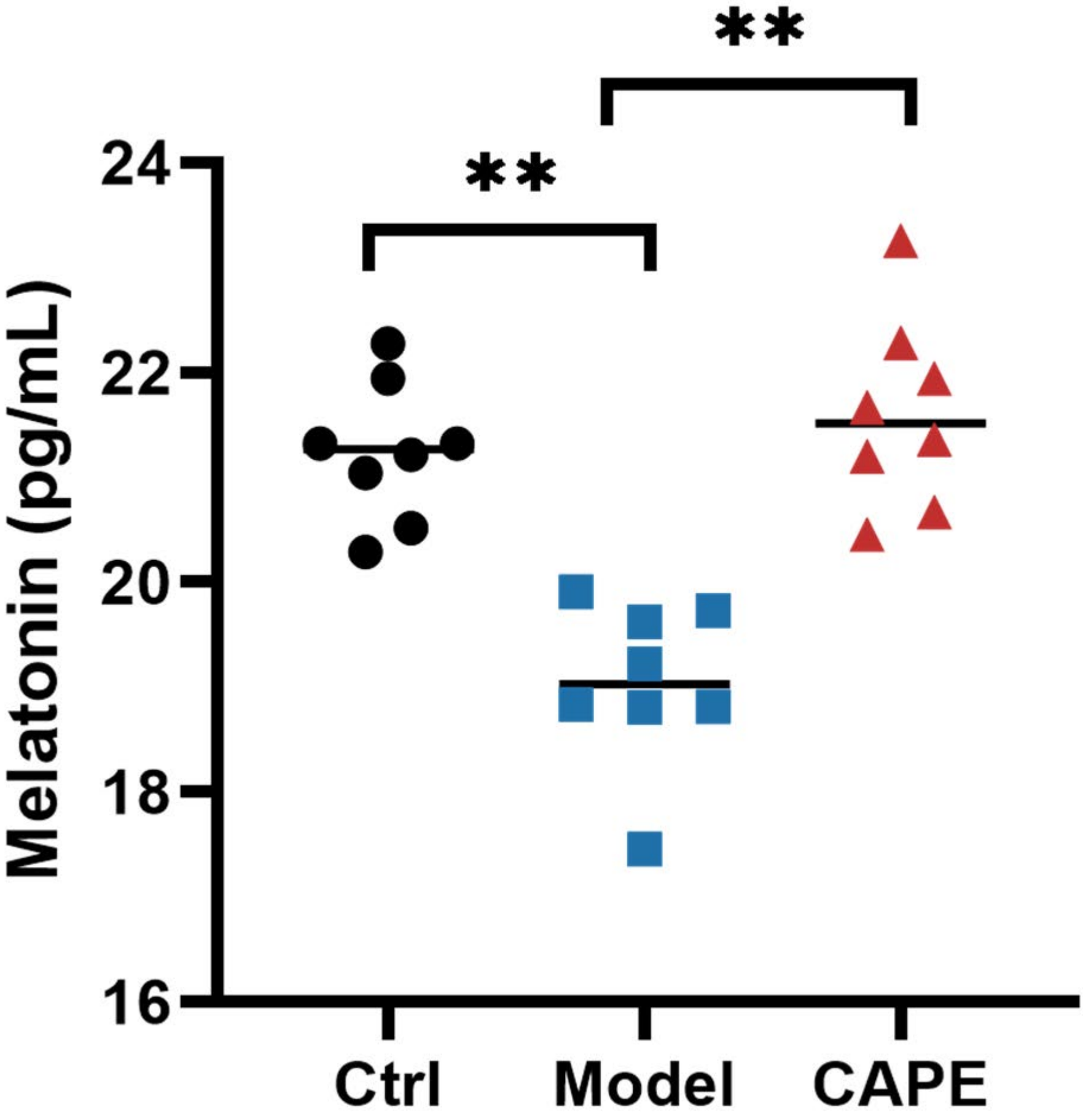
**
**
24
22
20
18
16
Melatonin (pg/mL)
Ctrl
Model
CAPE

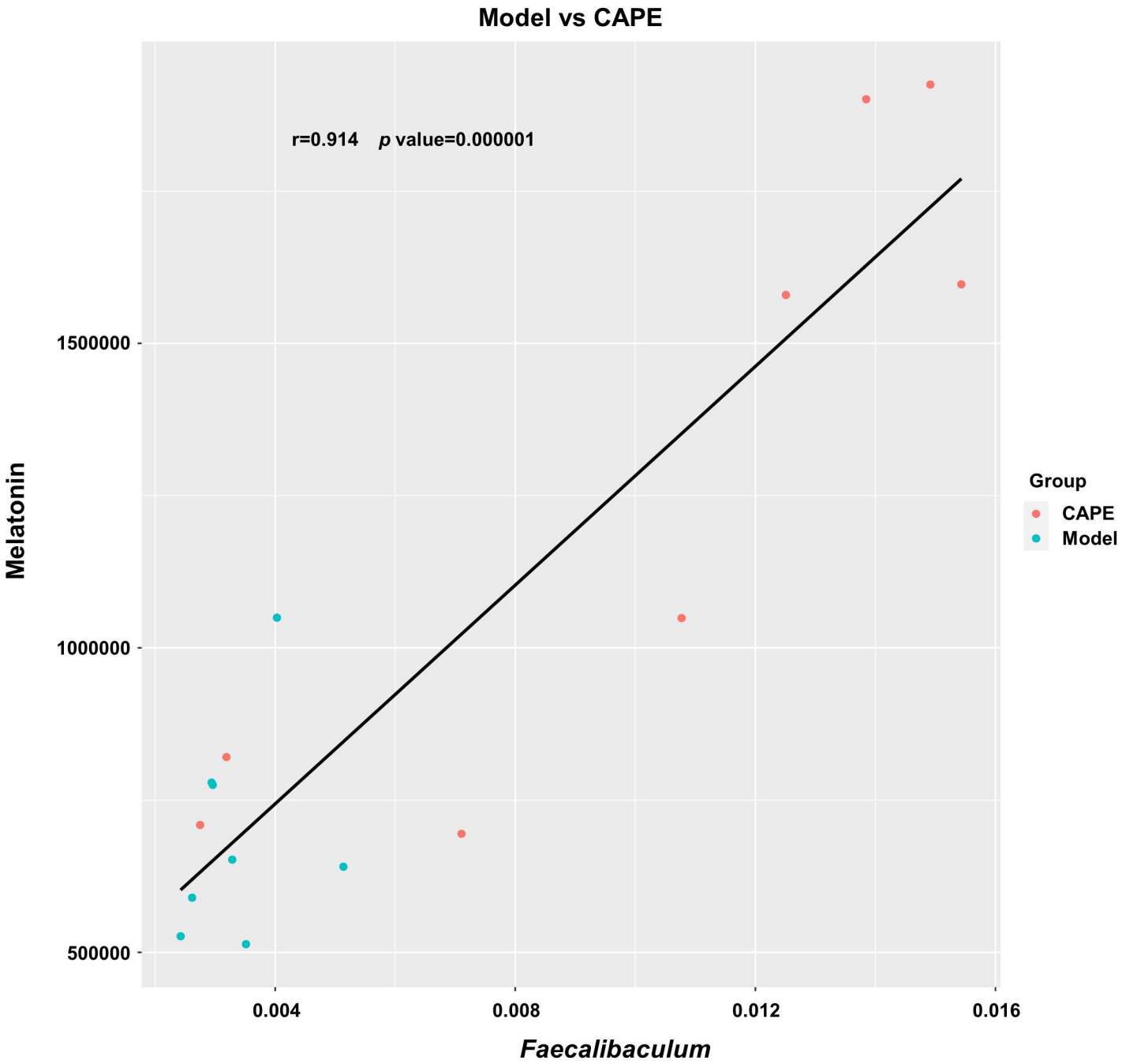
Model vs CAPE
r=0.914 p value=0.000001
Melatonin
1500000
1000000
500000
0.004
0.008
0.012
0.016
Faecalibaculum
Group
CAPE
Model